EUMETSAT

ROM SAF

RADIO OCCULTATION METEOROLOGY

ROM SAF CDOP-2

Visiting Scientist Report 32:

Preliminary investigation with GNOS bending angle data: Monitoring, quality control and possible implications for ROPP

Mi Liao

Danish Meteorological Institute (DMI)
European Centre for Medium-Range Weather Forecasts (ECMWF)
Institut d'Estudis Espacials de Catalunya (IEEC)
Met Office (METO)

Ref: SAF/ROM/DMI/REP/VS/32
Version: 1.0
Date: 17 May 2017

DOCUMENT AUTHOR TABLE

	Author(s)	*Function*	*Date*	*Comment*
Prepared by:	Mi Liao	ROM SAF Visiting Scientist	08/05/2017	
Reviewed by (internal):	Sean Healy	ROM SAF Scientist	15/05/2017	
Approved by:	Kent B. Lauritsen	ROM SAF Project Manager	07/06/2017	

DOCUMENT CHANGE RECORD

Issue/Revision	*Date*	*By*	*Description*
Version 0.0	08/05/2017	ML	First draft
Version 1.0	17/05/2017	ML	After reviewed by SBH

DOCUMENT DISTRIBUTION LIST

The VS report is made available at the ROM SAF website.

VS AUTHOR AND DURATION

VS Author

This VS study was carried out by Ms. Mi Liao, CMA, Beijing, China; Email: liaomi@cma.gov.cn

VS Duration

The VS study was performed during February – April 2017 at the ECMWF, Reading, UK with a short visit to Met Office, Exeter, UK.

ROM SAF

The Radio Occultation Meteorology Satellite Application Facility (ROM SAF) is a decentralised processing centre under EUMETSAT which is responsible for operational processing of GRAS radio occultation (RO) data from the Metop satellites and radio occultation data from other missions. The ROM SAF delivers bending angle, refractivity, temperature, pressure, humidity, and other geophysical variables in near-real time for NWP users, as well as reprocessed data (Climate Data Records) and offline data for users requiring a higher degree of homogeneity of the RO data sets. The reprocessed and offline data are further processed into globally gridded monthly-mean data for use in climate monitoring and climate science applications.

The ROM SAF also maintains the Radio Occultation Processing Package (ROPP) which contains software modules that aids users wishing to process, quality-control and assimilate radio occultation data from any radio occultation mission into NWP and other models.

The ROM SAF Leading Entity is the Danish Meteorological Institute (DMI), with Cooperating Entities: i) European Centre for Medium-Range Weather Forecasts (ECMWF) in Reading, United Kingdom, ii) Institut D'Estudis Espacials de Catalunya (IEEC) in Barcelona, Spain, and iii) Met Office in Exeter, United Kingdom. To get access to our products or to read more about the ROM SAF please go to: http://www.romsaf.org

Intellectual Property Rights

List of Contents

Executive Summary

This ROM SAF visiting scientist activity had three main objectives:

- Assess the quality of the GNOS GPS radio occultation (GPS-RO) bending angles by comparing with operational ECMWF short-range forecasts.
- Identify and investigate the cases that fail quality control with large bending angle departures.
- Document any GNOS specific problems using ROPP-PP and ROPP-FM modules, to guide future ROPP development.

We note that GNOS Beidou RO measurements are not investigated in this study.

The objectives of this activity have been completed successfully. The main results can be summarized as follows:

- We have identified and investigated the GNOS GPS-RO cases that fail quality control with large bending angle departures after processing with the ROPP software. The large departures can be attributed to the GPS L2 signal tracking problems which stop above 20 km in terms of tangent height, and the related L2 extrapolation. The percentage of the profiles with large departure is about 13~15%. A new L2 extrapolation approach was introduced in ROPP to solve the problem. It is based on the study of Culverwell and Healy (2016), introducing the corrected L2 bending angles produced by a Chapman layer model ionosphere, and the fitting relationship between L1 and L2. The new L2 extrapolation can effectively eliminate about 90% of the large departures. The remaining problems are mostly due to the L2 completely missing.

- We have studied and established the quality control methods suitable for GNOS GPS-RO profiles after correcting the large departures. A new L2 extrapolation, *noise_estimate*, can be taken as a QC parameter to evaluate the performance of the extrapolation. It is the standard deviation of the difference between the fit and observations above the extrapolated height. Mean phases delays of L1 and L2 at the height of 60 to 80 km tangent height are analysed and applied in the QC as well. The lowest SLTA of L2 is also set as a threshold to identify the bad profiles. Furthermore, the orbit height, or the variation of latitude and longitude for an occultation, is checked to avoid the retrieval process hanging in ROPP, although the odds are rather small. Using those parameters to form the QC method can identify 82.5% of the bad profiles whose mean bias is greater than 5%.

- We have assessed the quality of the GNOS bending angles by comparing with operational ECMWF short-range forecasts. GRAS profiles for the same time period are selected as a benchmark. The error statistics for the GNOS and GRAS bending angle profiles, in terms of the relative standard deviation, are similar at most of the heights, especially at the core range. The relative biases of the bending angles are almost the same below 20 km, but differ above 20 km. The setting and rising occultations of GNOS have biases of opposite sign. This needs to be investigated in the future.

• We have transformed the GNOS observations into BUFR format with 247 vertical levels, which can be easily ingested by the operational system of ECMWF. This guarantees the GNOS BUFR files distributed via GTS in the near future can be used by NWP centers.

The VS activity also documents the GNOS specific problems using ROPP-PP and ROPP-FM modules, to guide future ROPP development. It is recommended that the ROM SAF should:

(1) Add more inspections for the GNOS GPS L1 and L2 excess phase/SNR, and examine their SLTA, to access their observational quality at the stage of ROPP pre-process.

(2) Implement the new L2 extrapolation approach at the bending angle space, introduced by the current study, to improve the L2 bending angle extrapolation and eliminate large bias. Furthermore, carry out more sensitivity tests for the optimal fitting ranges of L1 and L2.

(3) Examine the variations of the latitude and longitude for an occultation. Profiles with abrupt shift magnitude should be stopped automatically in case of procedure stuck.

1. Introduction

1.1 Purpose of Document

This document contains the results from the ROM SAF Visiting Scientist activity on VS32 with the objectives to:

- Assess the quality of the GNOS bending angles by comparing with operational ECMWF short-range forecasts.
- Identify and investigate the cases that fail quality control with large bending angle departures.
- Document any GNOS specific problems using ROPP-PP and ROPP-FM modules, to guide future ROPP development.

Those objectives have been completed. The document is organized as follows: Section 1.2 briefly describes the background of the GNOS GPS-RO data and the processing, and Section 2 demonstrates the specific problems when using ROPP software. Section 3 is about the L2 extrapolation method dealing with the profiles which have large departures. Section 4 documents the QC methods suitable for GNOS. Section 5 shows the GNOS GPS-RO data performances comparing with ECMWF short-range forecast data. Section 6 is the conclusions and recommends.

1.2 Background

GNOS (Global Navigation Occultation Sounder) is on the FY-3C satellite, launched on Sep. 23rd, 2013. It is the first RO sounder on the Chinese polar orbiting meteorological satellite Fengyun series. It is also the first multi-GNSS RO receiver in orbit that can carry out RO measurements from both GPS (GPS-RO) and Chinese BDS signals. GNOS is manufactured by National Space Science Center (NSSC) of Chinese Academy Science (CAS), and is operated by the National Satellite Meteorological Center (NSMC) of the China Meteorological Administration (CMA). According to the Chinese Fengyun satellite programme, GNOS will be mounted on FY-3D (which will be launched around the third quarter of 2017) and the satellites following it. GNOS in the FY-3 series is expected to provide RO measurements continuously at least until 2030 (Yang et al., 2012).

As a multi-GNSS receiver, GNOS has the ability of tracking up to eight GPS satellites and four BDS satellites for precise orbit determination (POD). In addition, it has velocity and anti-velocity antennas for simultaneously tracking at most six and four occultations from GPS and BDS, respectively. Because of the presence of two antennas in opposite directions, both the rising and setting occultations can be retrieved. See more instrumental details in the table 1 and refer to Bai et al. (2014). Currently, FY-3C/GNOS receiving GPS signals can produce about 500 profiles per day for operational use, while GNOS from BDS signals have not been operational, and produce only about 200 profiles because of fewer reference satellites.

As with the pre-existing GPS-RO sounders (such as GPS/Met (Global Positioning System/Meteorology) experiment (Ware et al., 1996), CHAMP (CHAllenging Minisatellite Payload; Wickert et al., 2001), the Argentinian SAC-C (Satellite de Aplicaciones Cientificas-C; Hajj et al., 2004), the US/German GRACE (Gravity Recovery and Climate

Experiment) (Beyerle et al., 2005), the COSMIC (Constellation Observing System for Meteorology, Ionosphere, and Climate; Anthes et al., 2008), and the European Metop/GRAS (GNSS Receiver for Atmospheric Sounding) mission (Von Engeln et al., 2009)), the raw observations from GNOS consist of phase and SNR (signal to noise ratio) measurements. In addition, auxiliary information provided by the IGS (International GNSS Service), such as the GPS precise orbits, clock files, Earth orientation parameters, and the coordinates and measurements of the ground stations, are also needed. The IGS ultra rapid orbit products with an approximate accuracy of 10 cm in orbit are chosen for near-real-time operational use. LEO POD can be conducted by integrating the equations of celestial motion (Beutler, 2005) using the Bernese software v5.0 (Dach et al., 2007). The single difference technique is applied to obtain the excess phase as a function of time in an Earth-centred inertial reference frame. The Radio Occultation Processing Package (ROPP) software (V6.0), developed at ROM SAF (Radio Occultation Meteorology Satellite Application Facility), is used to determine different kinds of atmospheric parameters (Offiler, 2008). One-dimensional variational (1-D-Var) analysis, combined with the outputs of the T639L60 global forecast model, is used to retrieve temperature and humidity profiles. T639L60 is a global medium-range weather forecast system of China, which became operational at CMA in 2009. However, since early 2017, some changes were happened in our operational stream. We obtain the auxiliary files through ftp server in near-real-time provided by EUMETSAT GSN service, improving the timeliness within 3~4 hours. Besides, the POD software was replaced by the PANDA (Positioning And Navigation Data Analyst), which is developed originally by the Wuhan university of China (Shi et al, 2008).

Table 1 Main instrumental parameters for FY-3C/GNOS

Parameters	**FY-3C/GNOS**
Orbit Height	~836 km
Orbit Type	sun synchronous
Spacecraft mass	~750kg
Instrument mass	7.5kg
Constellation	GPS L1 C/A, L2 P BDS B1I,B2I
Channels	GPS：14 BDS：8
Sampling	POD 1Hz ATM.occ. (closed loop)50Hz ATM.occ.(open loop) 100 Hz ION occ. 1Hz
Open loop	GPS L1 C/A
Clock stability	1×10－12（1secAllan）
Pseudo-range precision	≤30cm
Carrier phase precision	≤2mm
Beam width of atmosphere occultation antenna	≥±30°(azimuth)

Using the original operational stream GPS-RO refractivity statistics are obtained in a preliminary check. Obviously some poor quality t data has to be filtered out (QC) based on the following rules: a profile is rejected if fractional refractivity greater than 0.1 occurs at more than 20 % levels in the profile. Besides, the outliers on a specific level are then excluded if they exceed the 3 sigma from a statistical point of view. As for standard deviation, the highest precision is from 5 to 25 km, smaller than 1 %. This is consistent with the results of previous validations for GPS-RO data (Kuo et al., 2004; von Engeln et al., 2009; Scherllin-Pirscher et al., 2011). Up to the height of 35 km, the standard deviation is still within 2 %, whereas above 35 km, the standard deviation starts to increase with height (Figure 1).

GNOS GPS-RO bending angle and refractivity products will be distributed via GTS very soon. Related preparation work has been completed and coarse quality controls are applied. In order to fully use GNOS data, more issues related to retrievals and quality control methods should be checked and implemented. As a new GPS-RO data source, GNOS is an ideal dataset to test the ROPP software.

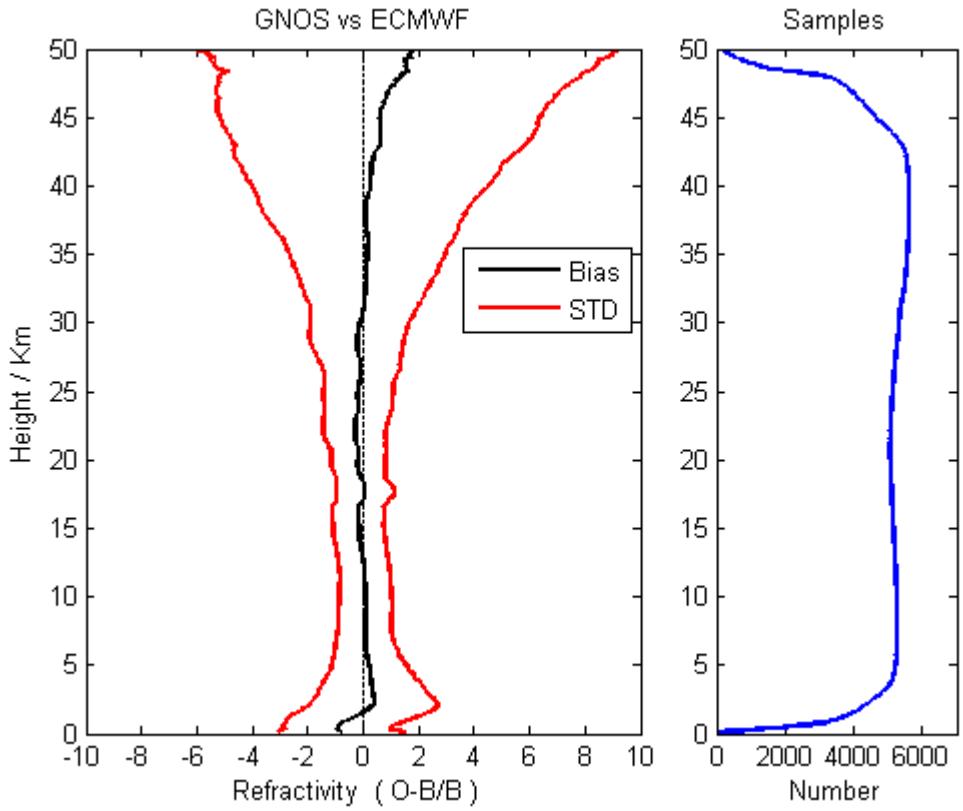

Figure 1. Refractivity deviation from the ECMWF reanalysis for GNOS GPS-RO (from 1 November to 31 December 2013). The left panel shows the mean bias (black) and the standard deviation (red), and the right panel shows the samples used vs. altitude.

2. GNOS specific problems using ROPP

2.1 L2 frequency extrapolation

From the excess phase to atmospheric parameters (such as bending angle, refractivity, dry temperature, temperature and humidity), GNOS applies the ROPP software for operational use. Through some preliminary assessments for the FY-3C/GNOS GPS-RO, the most obvious and prominent quality issue is the extraordinary bias, in the vertical range of 5-30 km and peaks at around 20 km (Figure 2). The percentage is about 13~15%. This phenomenon is not seen with other GPS-RO missions. It is most likely correlated with the GPS L2 signal tracking problems and the related extrapolation. As seen from Figure 3, the GPS L2 signal of those bad profiles stops mostly above 20 km in terms of SLTA (Straight Line Tangent Aptitude). Due to lack of observations, the L2 signal has to go through the extrapolation using a simple method, resulting in extraordinary biases below 35 km.

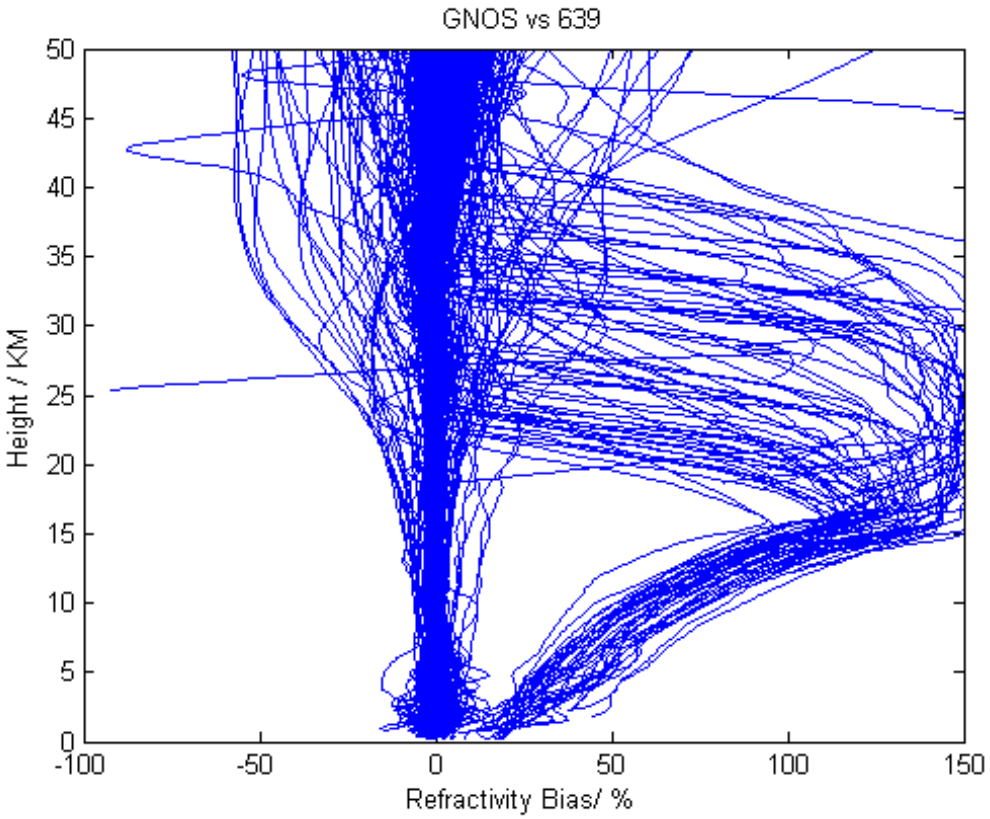

Figure 2. FY-3C/ GNOS GPS refractivity bias compared to T639 (the Chinese forecast model data), on 28th Jan 2017 with 489 samples

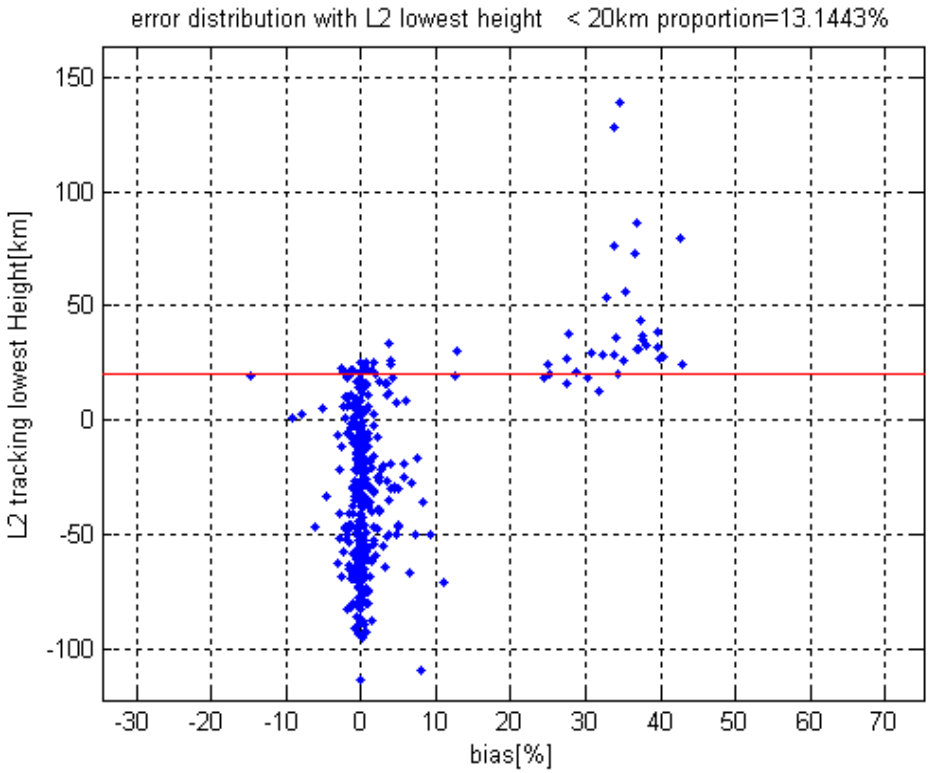

Figure 3. The bias versus the L2 lowest tracking height (Thanks to NSSC providing this figure)

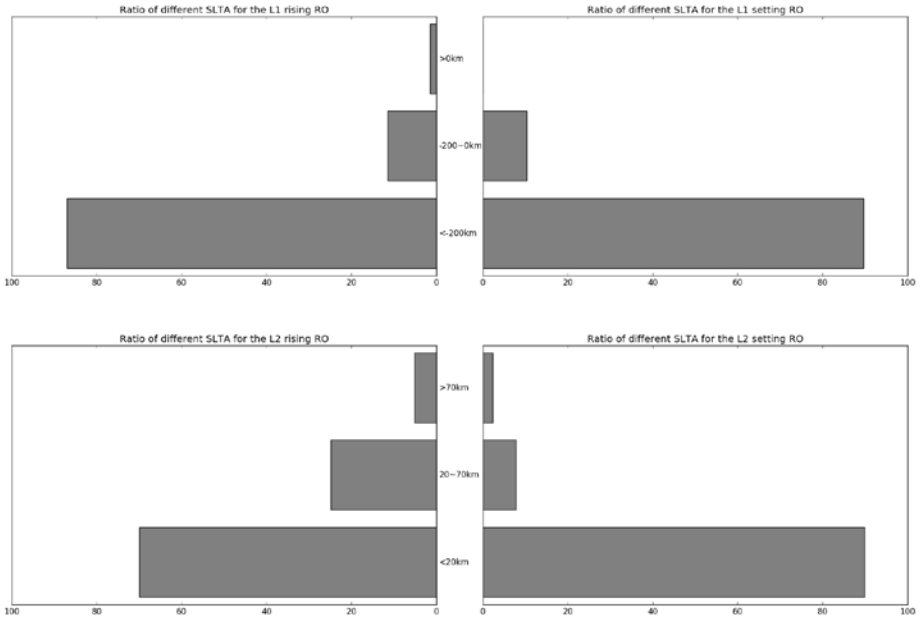

Figure 4. Ratio of different SLTA of the L1 C/A and L2 P for the rising and setting occultations, statistics result is from 28th Jan to 2nd Feb. 2017

Most of the bad cases are rising occultation, which is easy to understand. To improve the tracking in the lower troposphere and the rising occultation, open loop tracking is implemented for GNOS GPS L1 signal, but not for L2 (Ao et al. 2009). Under the complicated atmospheric conditions in troposphere, SNR falls. The GPS L2 signal is modulated by a pseudo-random precision ranging code (P code) for the purpose of anti-spoofing. Although GPS L2 can be demodulated using the semi-codeless method, it will be at the expense of SNR and precision (Kursinski et al., 1997). Therefore the performance of L2 signal tracking is not very good, especially for the rising occultation. Figure 4 is the SLTA percentages of L1 and L2 signal for the rising and the setting occultations,. It shows that there is no need to worry about the lowest tracking height of L1 C/A, either the rising or setting ones, and more than 98.5% profiles are below zero SLTA. However, as to the L2P, only 70% of the rising can get down below 20 km. There are 24.8% of rising profiles stop at the range of 20 ~70 km, and still 5.2% stopped above 70 km, almost means that no valid observations for the rising ones. 89.9% of setting occultations can get below 20 km, which is better than the rising, but about 10% stop above that height. Those profiles which have bad L2 signal observations tremendously affect the retrievals when using ROPP software to deal with GNOS data.

Figure 5 shows the performances in terms of excess phase, SNR, bending angle for two bad cases. It demonstrates a short time lasting of L2 excess phase and SNR both for the rising and setting occultation. For the two cases, there are no valid observations below 25 km or 30 km, respectively. But at the stage of bending angle, L2 is extending to the near surface. These bending angles are obtained by extrapolation. Because of lack of observations at the lower height, the bending angle of L1, L2 and LC starts to diverge due to improper extrapolation of L2. This kind of extrapolation leads to incorrect L2.

Fig 6 is the same plot but for two good cases, which L2 frequency gets 20 km SLTA. Compared with the bad cases, the good ones show longer observations for L2. Thus the bending angles of L1, L2 and LC are overlapped together, showing good consistency even at the lower part of the profiles.

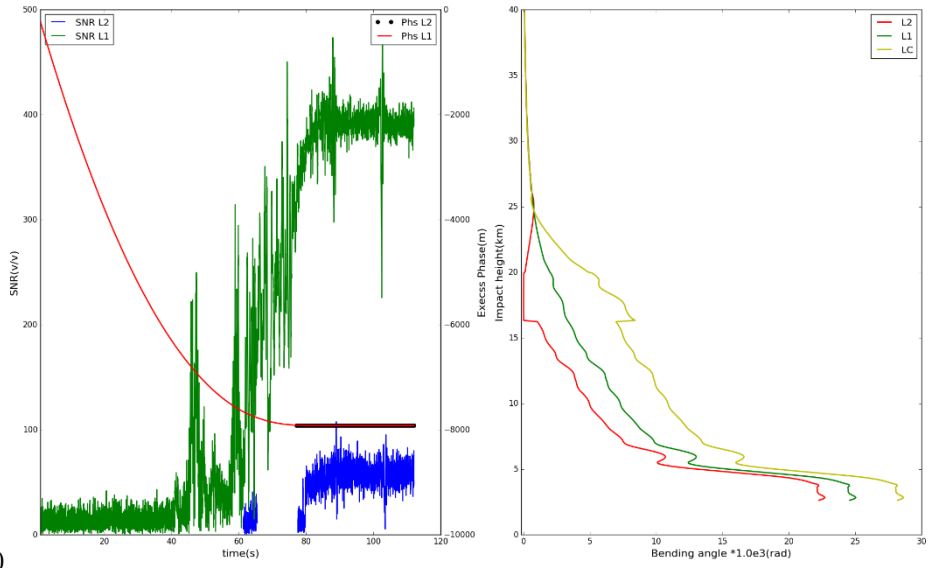

(a)

(b)

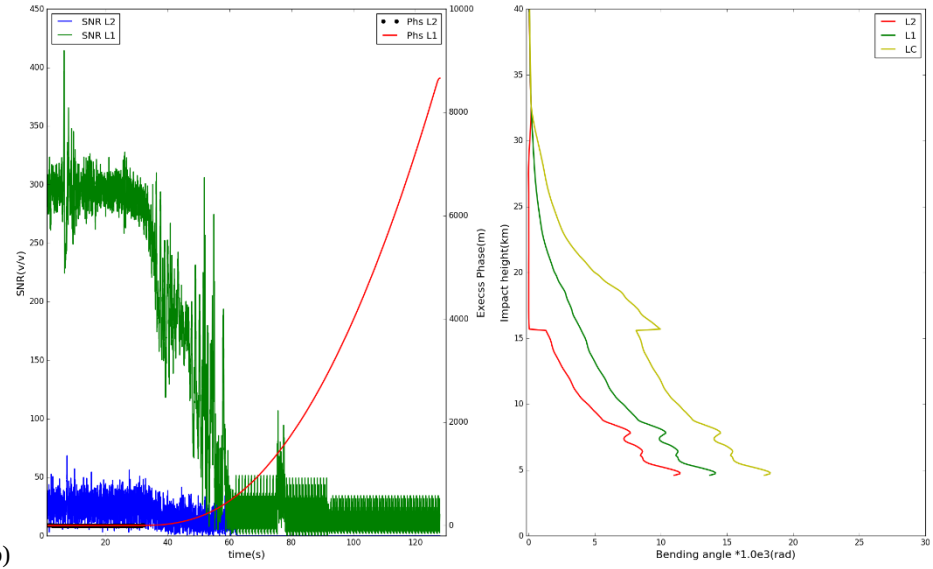

Figure 5. Two bad cases (a) A rising profile (FY3C_GNOSX_GBAL_L1_20170128_0332_AEG15_MS.NC), (b) a setting profile (FY3C_GNOSX_GBAL_L1_20170128_0850_AEG18_MS.NC). Example L1 (red) and L2 (black) SNR and excess phase measured data. The resulting L1 bending angle (green), L2 bending angle (red), and LC bending angle (yellow) profiles as a function of impact parameter computed using ropp_pp routines.

(a)

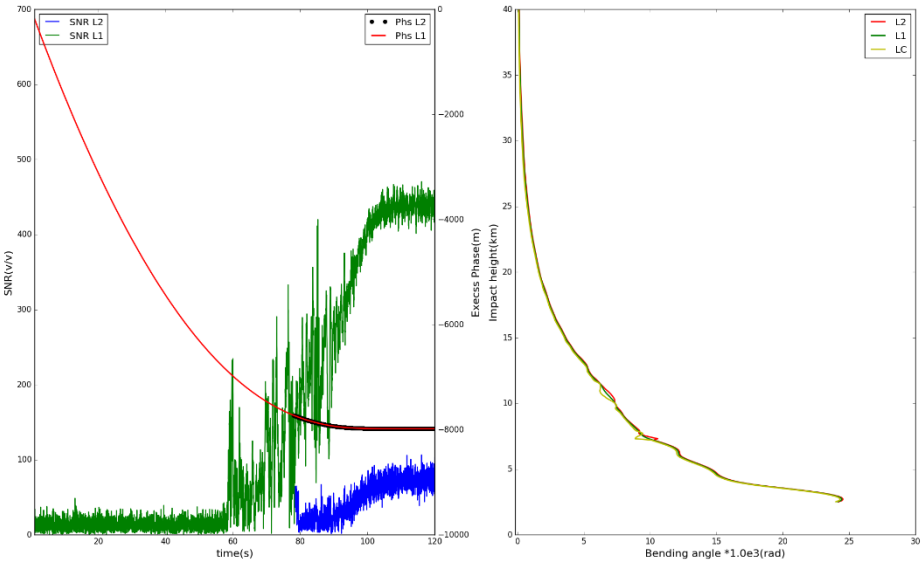

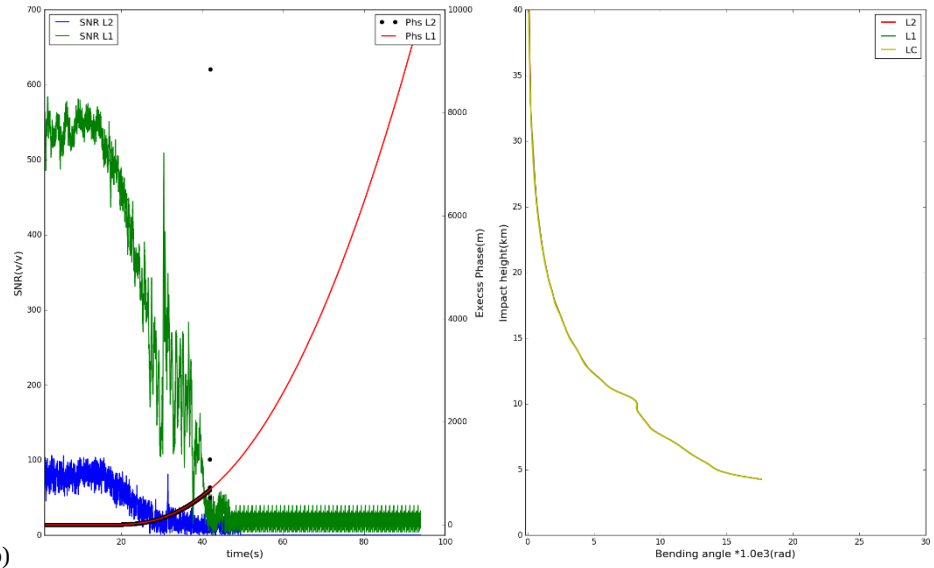

(b)

Figure 6. Two good cases (a) A rising profile (FY3C_GNOSX_GBAL_L1_20170128_1138_AEG27_MS.NC), (b) a setting profile (FY3C_GNOSX_GBAL_L1_20170128_1648_AEG31_MS.NC). Example L1 (red) and L2 (black) SNR and excess phase measured data. The resulting L1 bending angle (green), L2 bending angle (red), and LC bending angle (yellow) profiles as a function of impact parameter computed using ropp_pp routines.

2.2 Cases where ROPP "hangs"

There are few cases where ROPP_PP "hangs" during the retrieval process. In GNOS operational stream at CMA, these are killed after 30 minutes and the next profile is processed.

Take some examples to check this kind of issue closely. Figure 7 shows the altitude of LEO (specifically FY-3C) and its X, Y, Z coordination for a bad case. Its orbit range from the beginning to the end is about 20 km. Figure 8 is the normal one's performance, its orbit range is only about 2 km. Comparing the two figures, it can be seen that an abrupt change of the altitude of LEO occurred as to the bad case (Figure 7). Because of this, the SLTA and impact parameter of the bad case would be abnormal. The default value would be set after the *ropp_pp_preprocess* routine. During the process of Geometric Optics, error tolerance is big enough to process the bad case. However at the stage of Wave Optics, ropp_pp_monotonious.f90 hangs when the L2 impact parameter is NaN.

For a week's data, there are only three cases behaving like this. It is a small chance to get the abnormal LEO altitude, but the cases should be removed t. They can be easily detected by a simple quality control method implemented in the ROPP_PP. The reason for the abnormal orbit data needs to be investigated during the stage of POD.

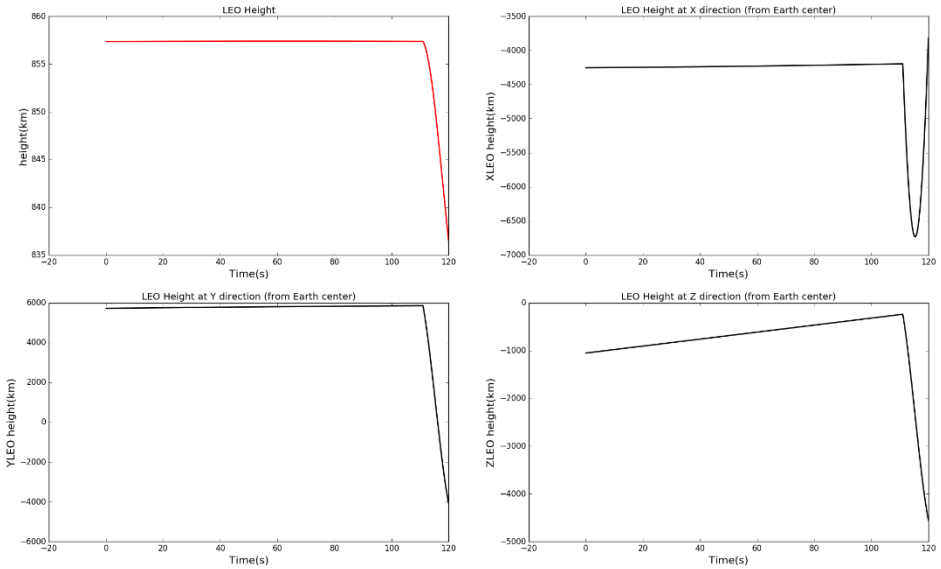

Figure 7. Bad case: Altitude of LEO (specifically FY-3C) and X, Y, Z coordination as a function of time (FY3C_GNOSX_GBAL_L1_20170222_0037_AEG28_MS.NC)

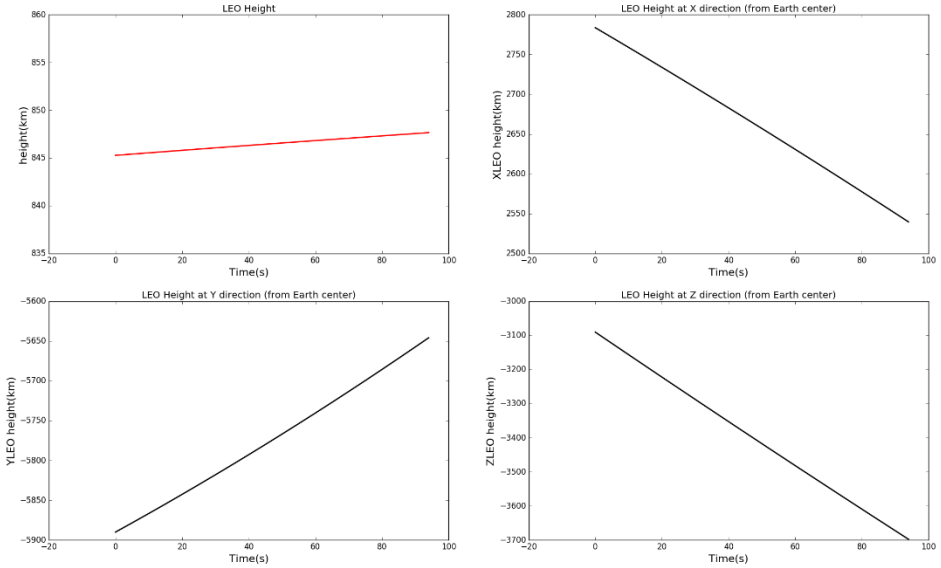

Figure 8. Normal case: Altitude of LEO (specifically FY-3C) and X, Y, Z coordination as a function of time (FY3C_GNOSX_GBAL_L1_20170216_0009_AEG31_MS.NC)

3. New L2 extrapolation

As mentioned in the section 2.1, some sort of extrapolation of the observed L2 signal is required before it can be combined with the L1 signal in order to remove the ionospheric contribution to the bending. However, the current L2 extrapolation implemented in ROPP leads to obvious errors when processing GNOS GPS-RO data. Therefore, another L2 extrapolation method should be applied in the ROPP to solve the problem. Culverwell and Healy (2016) modelled the bending angles produced by a Chapman layer model ionosphere and established some basic theory for the relationship between fitting L1 and L2.

For a vertically localized region of refractivity, sited well above tangent points of interest, the ionospheric contribution to the bending angle at frequency f can be simply expressed by:

$$\alpha(a) = 2a\frac{k_4}{f^2}\int_a^{\infty}\frac{xn_e(x)}{(x^2-a^2)^{\frac{3}{2}}}dx \qquad \text{(See SAF/ROM/RSR/017 eq. 2.6)} \quad (3.1)$$

Where α is the bending angle, a is the impact parameter, f is the frequency, $x = nr, k_4 = \frac{e^2}{8\pi^2 m_e \varepsilon_0} = 40.3m^3s^{-2}$ and n_e is the electron number density. Commonly, the electron number density can be expressed in terms of the vertically integrated total electron content, TEC, which is defined as $TEC = \int n_e dr$. So the equation above can be written as:

$$\alpha(a) = 2a\frac{k_4}{f^2}TEC\frac{r_0}{(r_0-a^2)^{\frac{3}{2}}} \quad (for\ a < r_0) \quad \text{(See SAF/ROM/ RSR/017 eq. 3.2)} \quad (3.2)$$

r_0 is the peak height of the Chapman layer, ideally, it could be taken as 300 km.

As to the GPS L1 and L2 frequency, their difference is expressed as:

$$\alpha_2(a) - \alpha_1(a) = 2ak_4TEC\left(\frac{1}{f_2^2}-\frac{1}{f_1^2}\right)\frac{r_0}{(r_0-a^2)^{\frac{3}{2}}} \quad (3.3)$$

If we take $x_{so} = 2ak_4TEC\left(\frac{1}{f_2^2}-\frac{1}{f_1^2}\right)$, then

$$\alpha_2(a) = \alpha_1(a) + x_{so}\frac{r_0}{(r_0-a^2)^{\frac{3}{2}}} \quad (3.4)$$

x_{so} is the least-square fit based on observed L1 and L2 bending angles, which tries to fit the shape of ionospheric bending model.
The difference between L2 and L1 shows a sort of function in Figure 9. It is the lower part of the ionospheric bending model. The extrapolation of L2 bending angle can be obtained with L1 and the second part of eq. 3.4 if x_{so} is a fit based on the L1 and L2 observations in a 20 km interval. For example, if the L2 observations stops around 30 km, x_{so} is fit through the information between 30 km and 50 km. Then the L2 bending angle below 30 km can be extrapolated by the L1 plus the fitted x_{so}. Here we set an experienced value for the top height, as we don't think the L2 extrapolation could perform very well if it fits observations above 70 km.

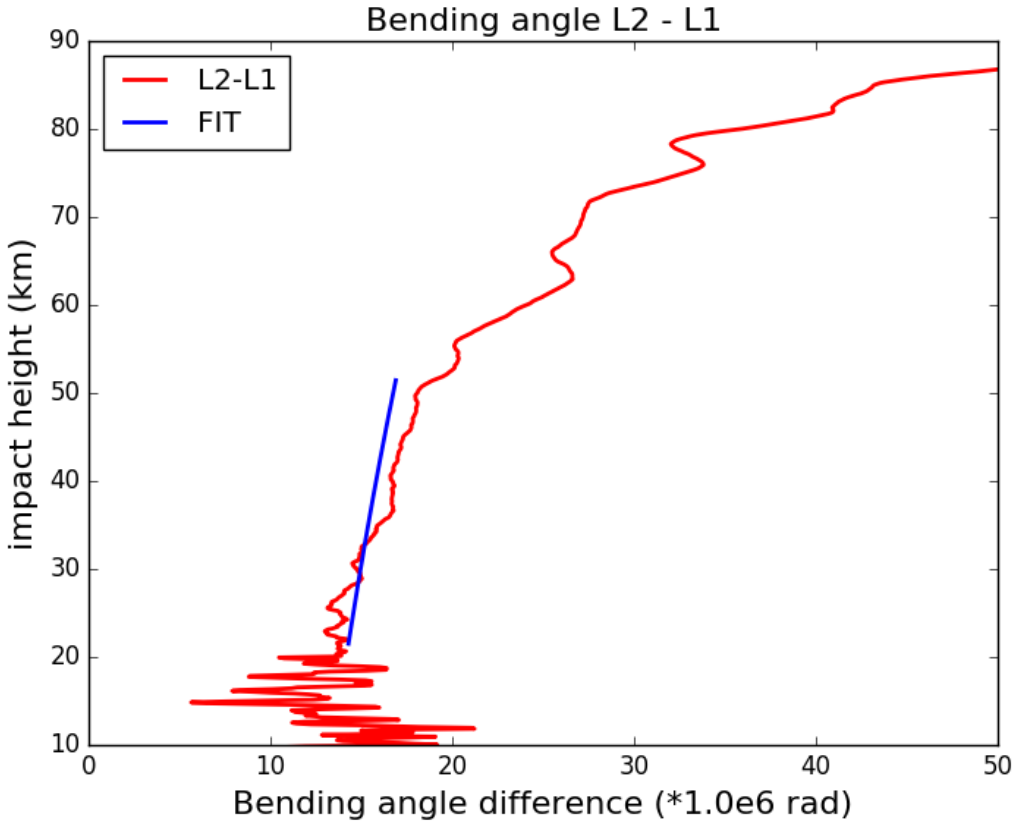

Figure 9. The difference of bending angle between L2 and L1, and the least-square fit from 20 to 50 km

Five bad profiles whose L2 signal stops above 20 km in terms of SLTA were chosen for studying the extrapolation method. Their detailed information is listed in table 2. Because the ionospheric effect becomes smaller in relative terms with the height decreasing, the magnitude of bending at different frequencies would become closer and closer. Seen from the direct comparisons between the new and the old extrapolation results of case 1 (Figure 10), L2 is very different to L1 before correction. After applied the new extrapolation approach, L2 bending angles below 20 km are consistent with L1 and LC as well. More cases can be found from Figure 11 to 14. It is concluded that a more reliable linear correction bending angle can be obtained by using the new L2 extrapolation approach than the original L2 extrapolation method implemented in ROPP.

Table 2. Details of the selected five bad occultations

No.	Occ. time (yymmdd.hhmm)	Longitude (degree)	Latitude (degree)	Occ. direction	SLTA_L2 (km)
1	170128.0332	-99.154	25.070	rising	21.917
2	170128.0740	24.705	-4.222	rising	25.793
3	170128.0850	-177.178	21.596	setting	30.173
4	170128.1346	113.585	45.390	rising	26.468
5	170128.1638	-143.664	-55.377	setting	23.236

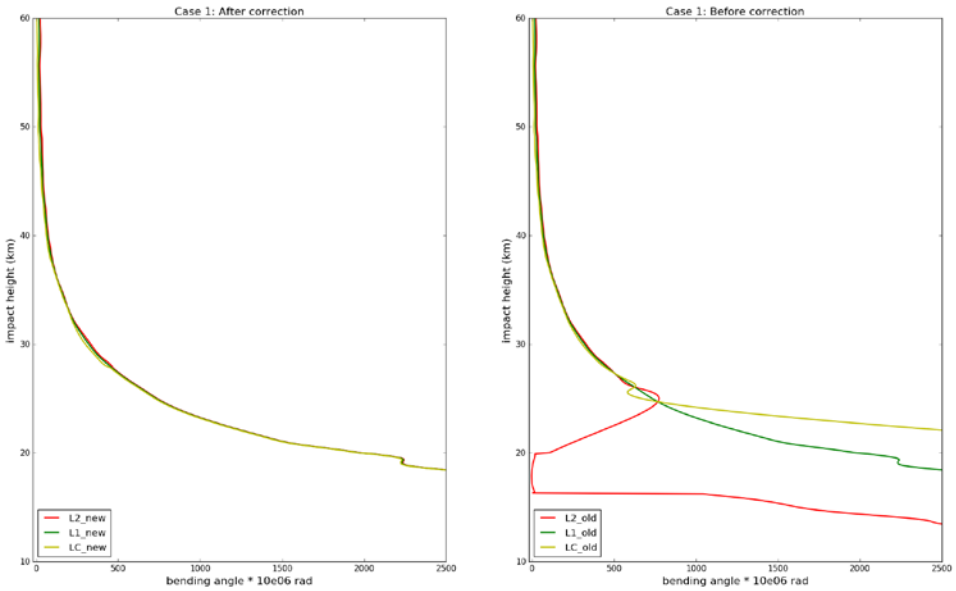

Figure 10. Case one: the bending angle of L2 (red), L1 (green) and LC (yellow) before (right) and after (left) correction

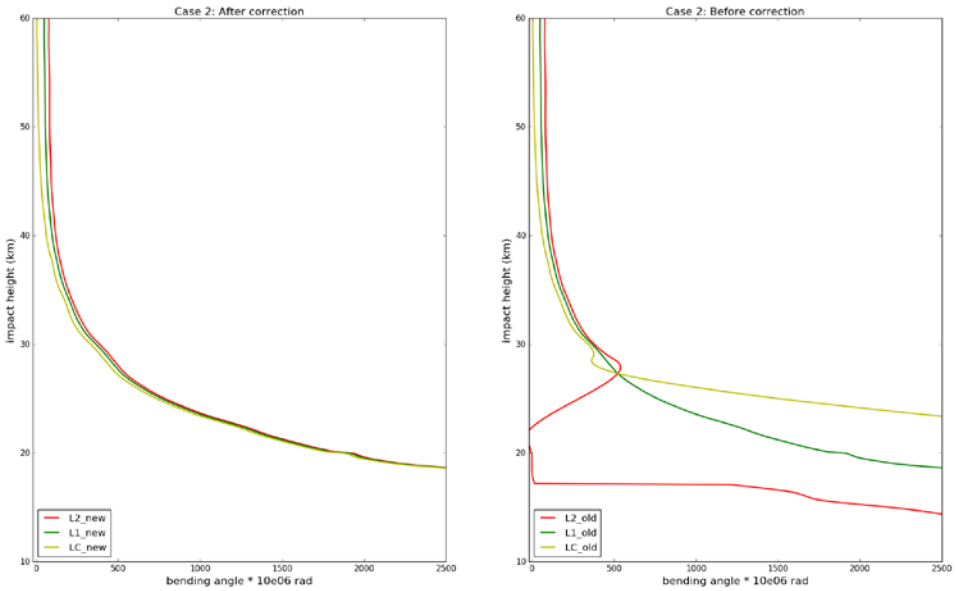

Figure 11. The same as Figure 10 but for case two

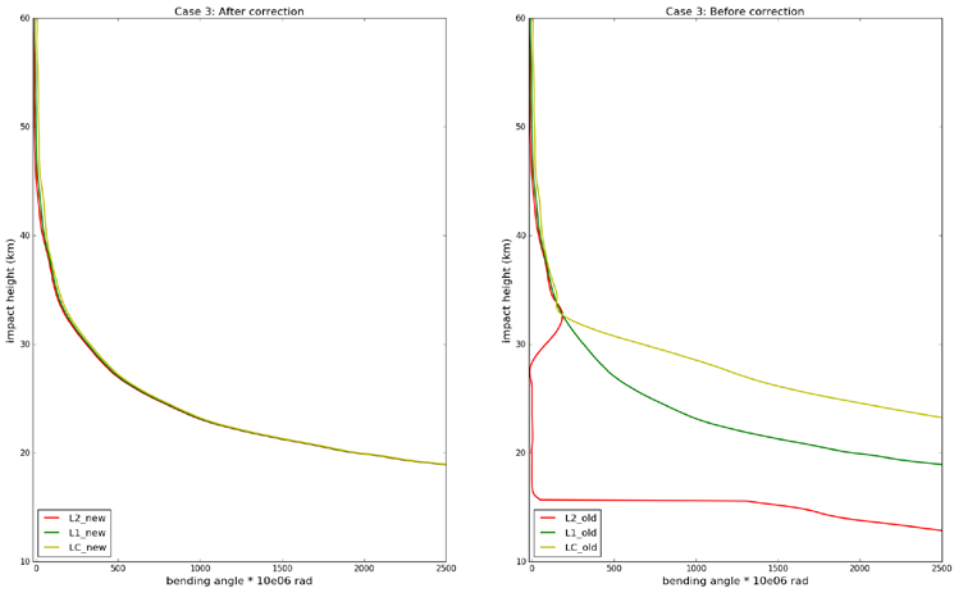

Figure 12. The same as Figure 10 but for case three

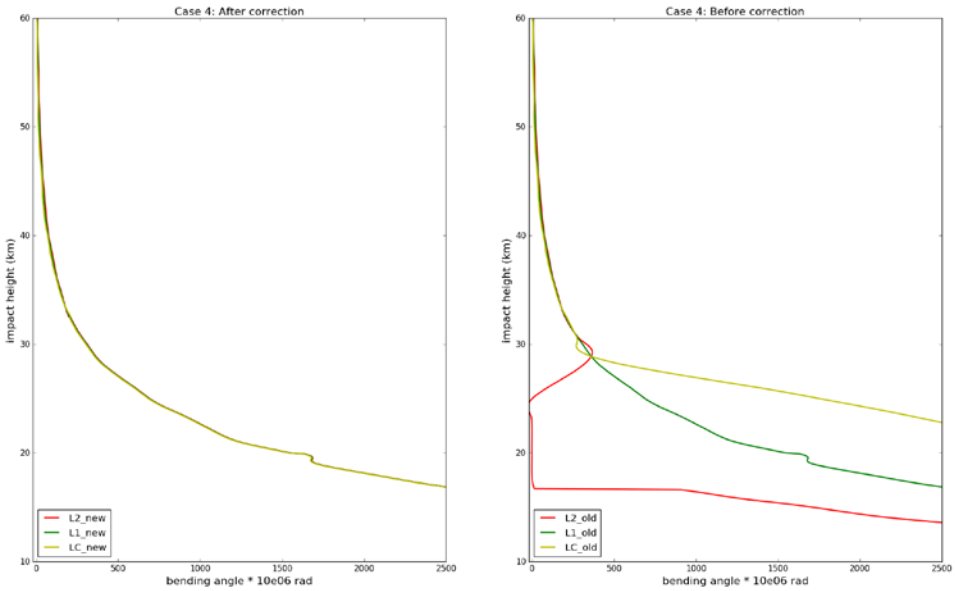

Figure 13. The same as Figure 10 but for case four

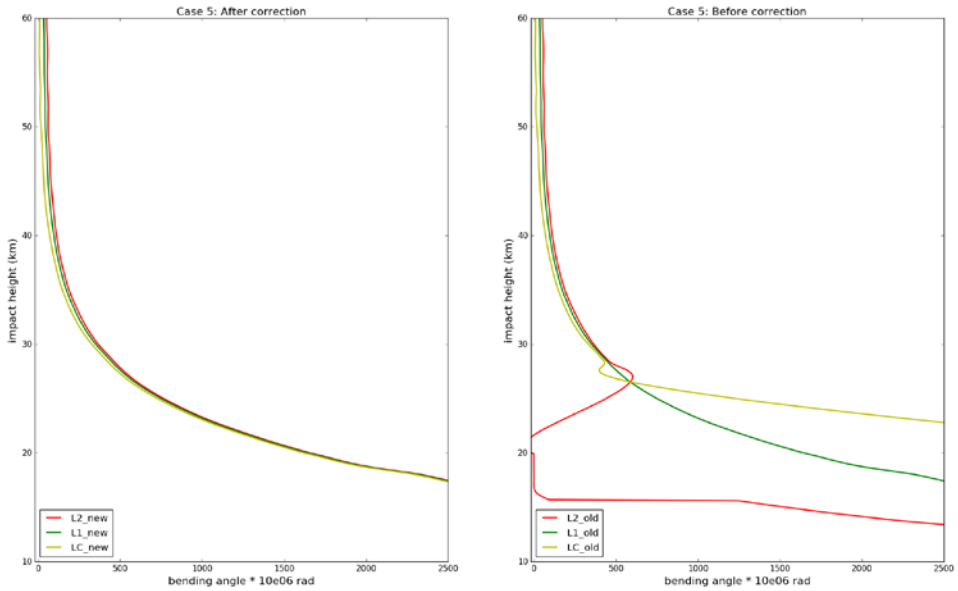

Figure 14. The same as Figure 10 but for case five

Table 3. Details of the four good profiles

No.	Occ. time (yymmdd.hhmm)	Longitude (degree)	Latitude (degree)	Occ. direction	SLTA_L2 (km)
1	20170128.0103	149.508	-38.445	rising	4.011
2	20170128.0251	70.857	-51.463	rising	12.928
3	20170128.0814	7.240	-70.147	setting	-62.296
4	20170128.1138	147.389	-48.192	rising	-24.538

Obviously, using the new simple ionospheric model for the t the L2 extrapolation performs very well for the bad profiles with large bias. But how does the new extrapolation method affect normal cases? Here the normal profiles are defined as the lowest SLTA reaching below 20 km, and the mean standard deviation to the reanalysis data is within 2% from surface to 35 km. Therefore, four good profiles (Table 3) are selected to test the new extrapolation.

Generally speaking, the new extrapolation method does not degrade the good profiles, seen from Figures 15 to 18. On the contrary, the new method can smooth some occultation points and improve the consistency of L1 and L2. Just as the case one (figure 15), the old L2 encountered two small leaps during the height of 10 to 16 km, and result in LC leaps as well (Figure 15), but the new L2 and LC performs more smooth. The same happens to the case four, but at the height of 6 to 12 km (Figure 18). Case two only has one leap around the height of 20 km (Figure 16). Thus, the new method can remove the leaps if there are any, and produce smoother LC bending angle profiles.

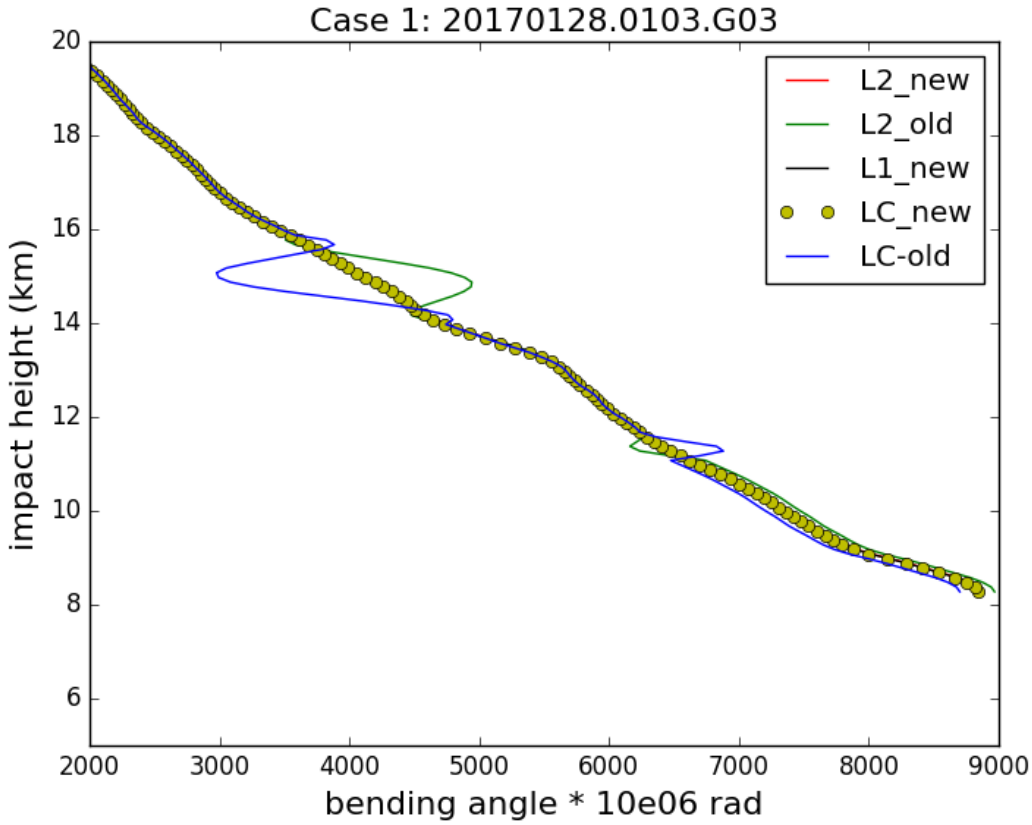

Figure 15. Good case one: the bending angle of L2, L1 and LC before and after correction

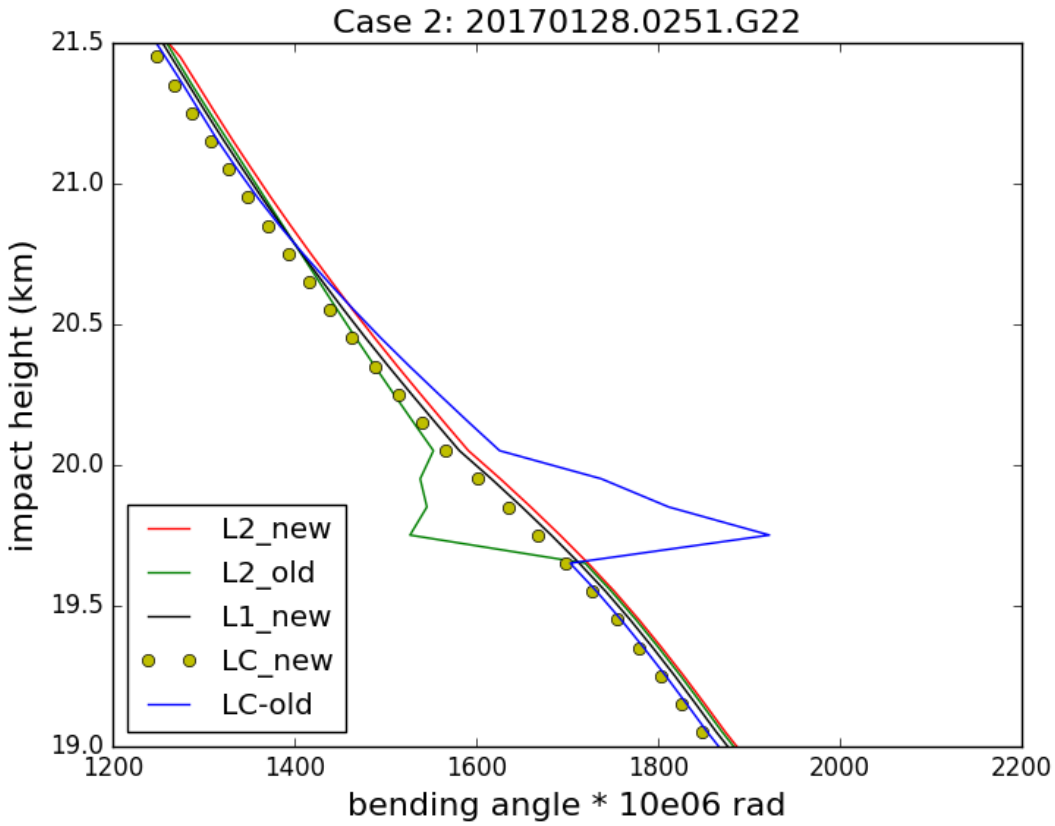

Figure 16. Good case two: the bending angle of L2, L1 and LC before and after correction

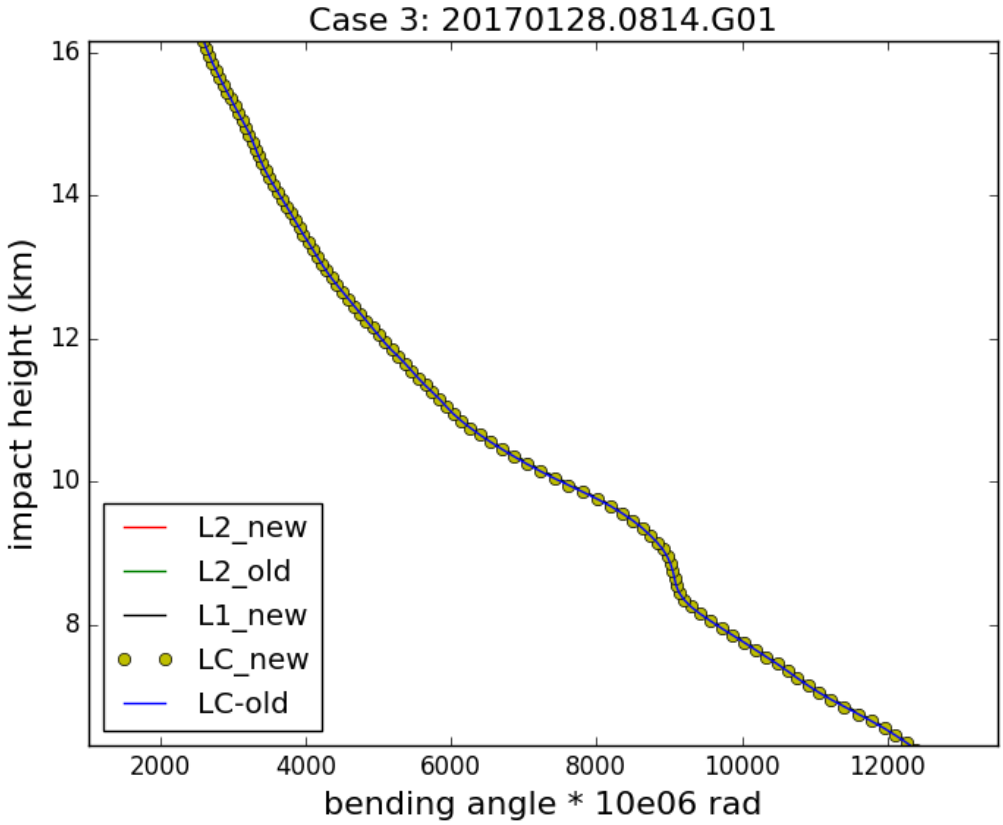

Figure 17. Good case three: the bending angle of L2, L1 and LC before and after correction

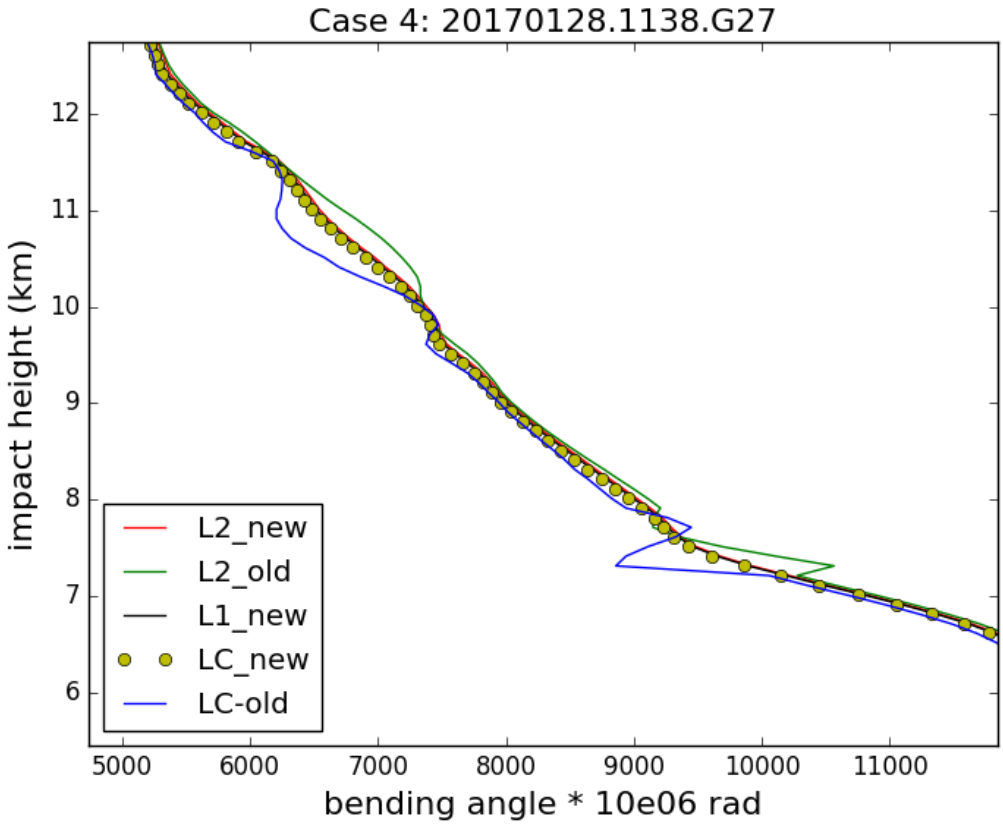

Figure 18. Good case four: the bending angle of L2, L1 and LC before and after correction

A simple way to demonstrate the extrapolation methods is to compare their refractivity retrievals with the forecast model data. One day of data was used to test the new L2 extrapolation method. Figure 19 shows that the new method can effectively eliminate most of the branches (~90%). Eight profiles still have a large bias, because their L2 SLTA stop above 70 km, which are out of the processing range used in the extrapolation (below 70 km).

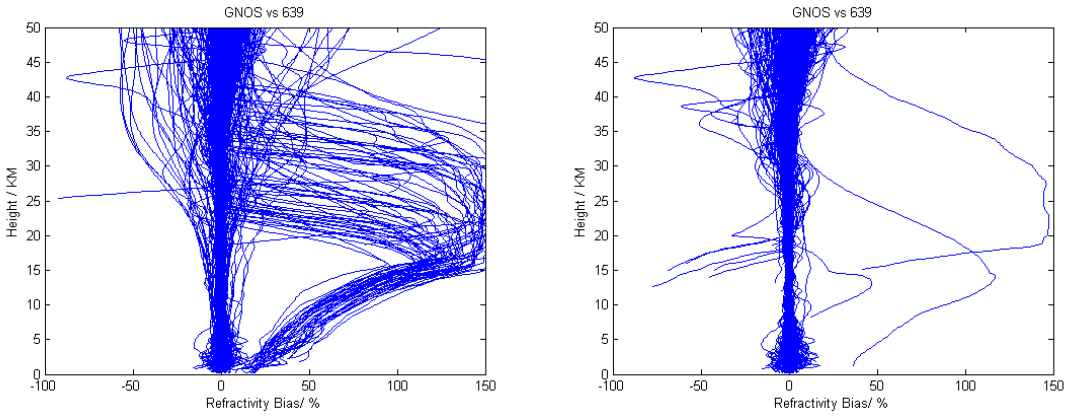

Figure 19. FY-3C/ GNOS GPS refractivity bias compared to T639 (the Chinese forecast model data), on 28th Jan 2017 with 489 samples. The left is the result of the original GNOS GPS data, and right is the result of GNOS GPS after the new L2 extrapolation approach.

4. Quality control methods

Although the new L2 extrapolation method removes more than 90% poor quality profiles, there are still some profiles with obvious errors. Some internal QC methods need to be implemented. Based on the GPS-RO error sources and characteristics, many internal QC methods are proposed. For example, CDAAC applied the altitude Z below which a low quality of L2 signal has been detected, the maximum difference of Ll and L2 bending angle above Z, the ionospheric scintillation index analysed from the amplitude of L1 signal at high altitudes, and so on [Kuo et al., 2004]. Gorbunov [2002] proposed a QC procedure in terms of the analysis of the amplitude of the GPS-RO data transformed by the Canonical Transform (CT) or the Full Spectrum Inversion (FSI) method, which is useful to catch the corrupted data because of phase lock loop failures. Beyerle et al. [2004] also suggested a QC approach to reject the GPS-RO observations ruined by ionospheric disturbances according to a parameter R defined by the phase delay of L1 and L2 signal.

In light of the characteristics of GNOS GPS-RO data, we tested and established some new internal QC methods to detect the poor quality profiles.

4.1 Noise estimate of the L1 and L2 fit

Due to L2 signal tracking problems, 15% profiles would be degraded. After applying the new L2 extrapolation method, most of them can be effectively corrected. As seen from the formula 3.4, the key of correction is how well the *x_so* fits the difference of L1 and L2 bending angle in a 20 km interval in the range between 20 km to 70 km. Currently, 20 km or the minimum L2 SLTA is the lower limit of the fitting interval.

We have introduced a new parameter, *noise_estimate*, to test the fit in the 20 km interval. It can be expressed as:

$$noise_{\_estimate} = \frac{\sqrt{\sum(x_{so} * \frac{r_0}{(r_0 - a^2)^{\frac{3}{2}}} - \Delta\alpha(a))^2}}{n} * 10^6 \quad (4.1)$$

Where $\Delta\alpha$ the difference of L1 and L2 bending angle and the sum is is over the fitting interval.
The physical meaning of *noise_estimate* is easy to understand, because it evaluates standard deviation of the difference between the fit and observations. If the *noise_estimate* is small enough, thus x_{so} is fitted well, then the L2 extrapolation using the $x_{so}$is probably adequate.

After accumulating seven days of data, a histogram of the *noise_estimate* can be obtained and it obviously demonstrates where the appropriate threshold should be (Figure 20). If the value of the *noise_estimate* is greater than 20 micro-radians, the profiles will be rejected. As we set the highest altitude of the new extrapolation method at 70 km, the profiles whose SLTA stop above that height would not be corrected, and their *noise_estimate* can be set as a default such as 99.0. Therefore, the *noise_estimate* threshold can detect those profiles as well.
We have used one day of data to test the performance of the *noise_estimate* as a QC parameter. The good profiles are defined as the mean biases from surface to 50 km are

within 5%, otherwise, the bad profiles are greater than 5%. Figure 21 shows that the *noise_estimate* of the good profiles are highly focused on the values are below 20; while the *noise_estimate* of the bad profiles are distributed from 0 to the largest. It demonstrates that the *noise_estimate* parameter setting threshold at 20 can mostly identify the good ones and some part of the bad ones, but some bad ones could be missed. This parameter can be used as one factor, but still other parameters are needed to complete the QC.

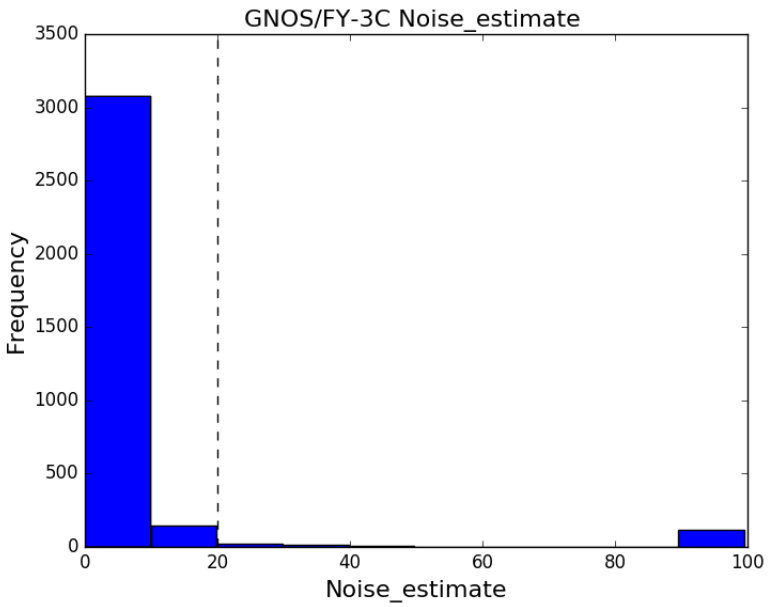

Figure 20. The histogram of the *noise_estimate* parameter using seven days of data from 16th Feb. to 22nd Feb 2017

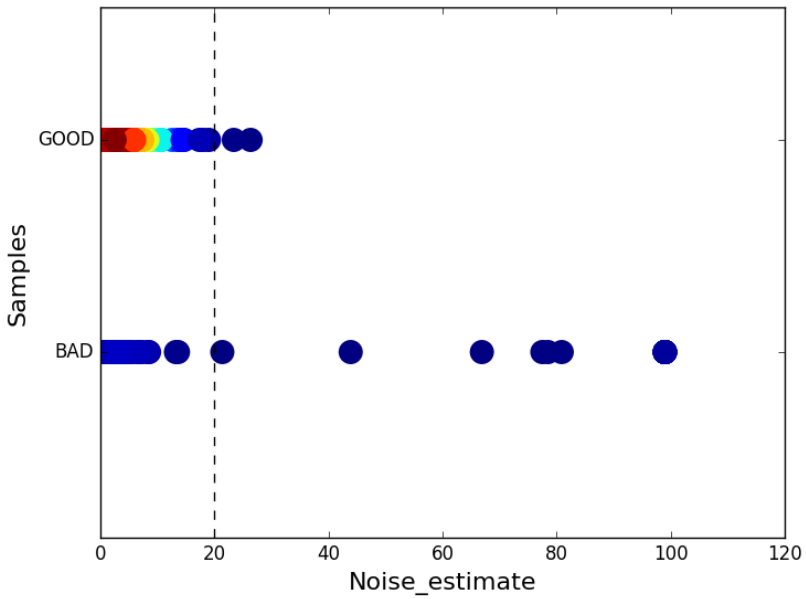

Figure 21. The *noise_estimate* versus the good and bad samples (28th Jan 2017). Different colour represents different overlapping density, the dark blue is the lowest and the dark red is the highest, the colours between them show gradually higher density.

4.2 SNRs and Mean delay phase of L1 and L2

As seen from the previous section, the *noise_estimate* QC parameter does not detect all the poor quality profiles. We need extra quality control methods to identify them. Therefore, it is necessary to closely check the performance of GNOS GPS-RO data in terms of SNRs and mean phase delays, which can also show the observational quality of GPS-RO data.

Weak SNRs at the height of 60 to 80 km can reflect the observational quality. Therefore, the SNR and the delay phase of L1 and L2 have been examined in terms of histograms. As seen from Figure 22, the threshold can be set at 200. However, from the Figure 23 which shows the test of performance, it is hard to cut off the good profiles or bad ones with one threshold. The same situation happens in the L2 SNR (Figure 24, 25). Therefore, we do not suggest applying the L1 and L2 SNR as the QC parameters when processing the GNOS GPS-RO data. Figure 26 to Figure 29, which are the histograms and the performance test of the L1 and L2 mean delay phase in rising occultations, there is certainly relationship between the poor profiles and the mean delay phase of L1 and L2. Combined with L1 and L2 rising occultations, if their values are greater than - 150 at the same time, most of the bad profiles can be identified. Unavoidably, a few of the good profiles could be wrongly detected as well and few bad ones could be missed. The statistical performance will be demonstrated in Section 4.5.

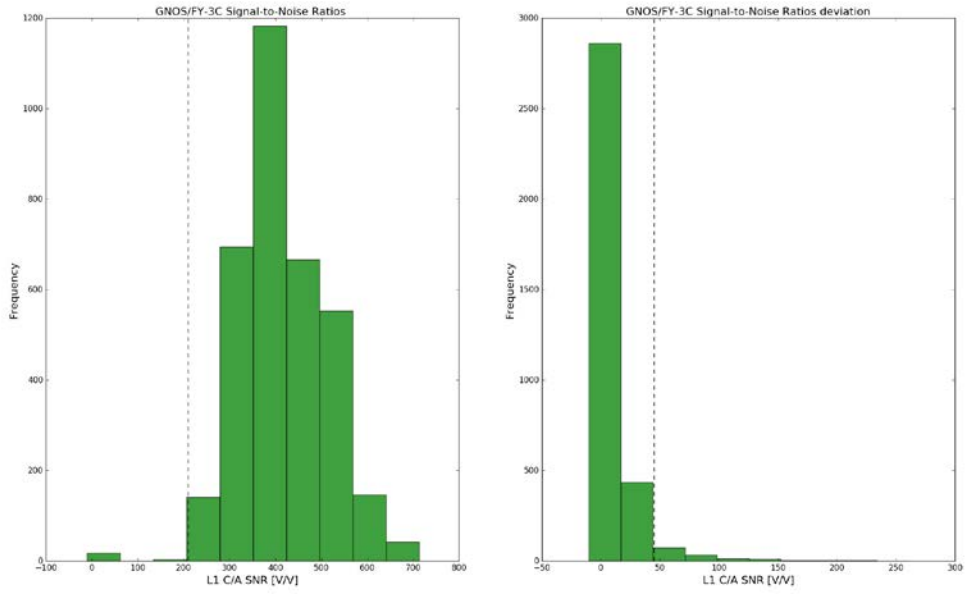

Figure 22. The histograms of the L1 SNR and its SNR std. using seven days of data from 16th Feb. to 22nd Feb 2017

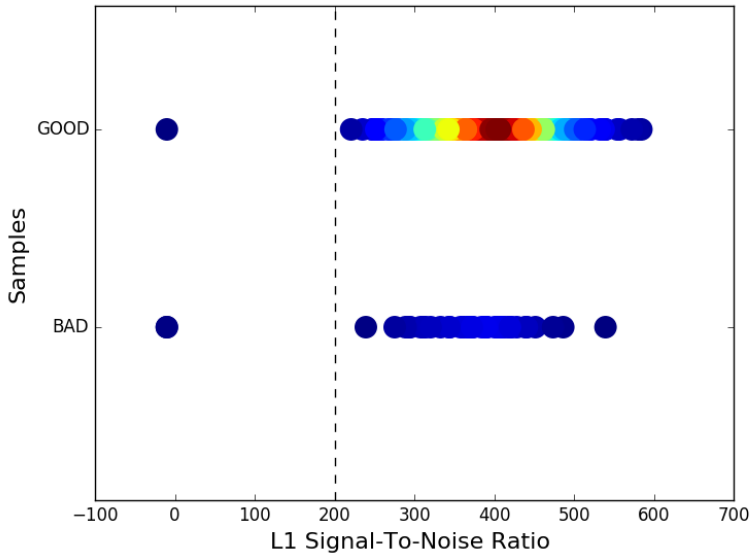

Figure 23. The L1 SNR versus the good and bad samples (28th Jan 2017). Different colour represents different overlapping density, the dark blue is the lowest and the dark red is the highest, the colours between them show gradually higher density.

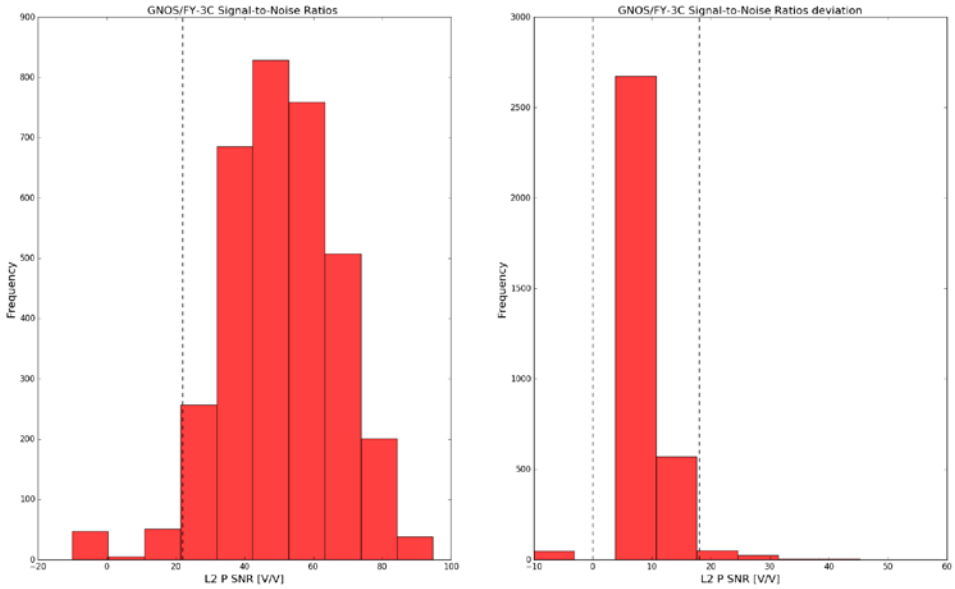

Figure 24. The histograms of L2 SNR and its SNR std. using seven days of data from 16th Feb. to 22nd Feb 2017

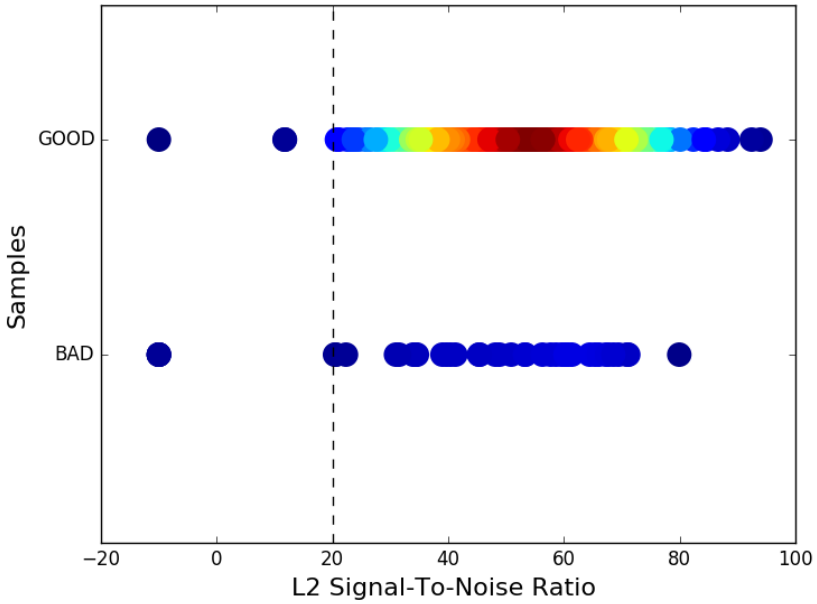

Figure 25. The L2 SNR versus the good and bad samples (28th Jan 2017). Different colour represents different overlapping density, the dark blue is the lowest and the dark red is the highest, the colours between them show gradually higher density.

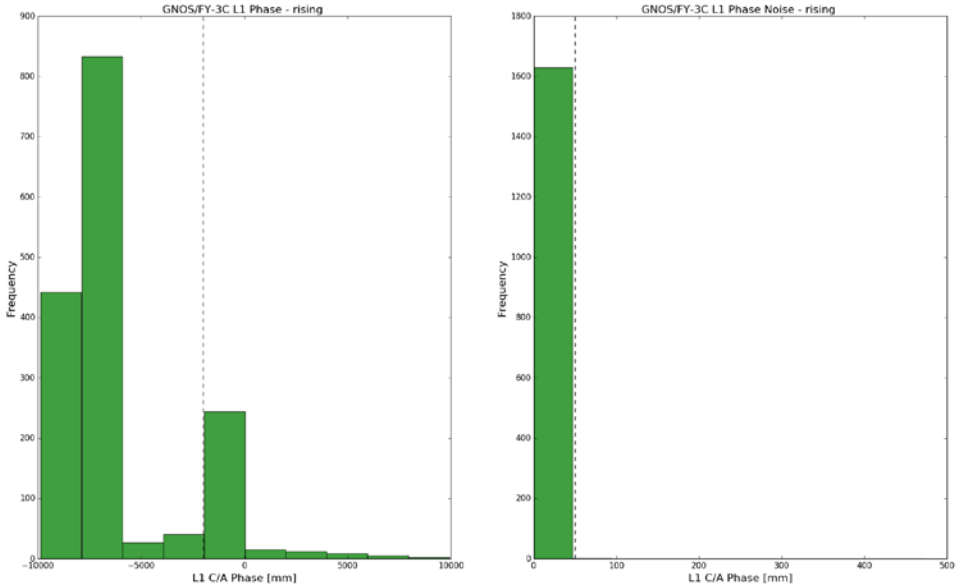

Figure 26. The histograms of L1 mean phase delay and its std. for the rising occultation using seven days of data from 16th Feb. to 22nd Feb 2017

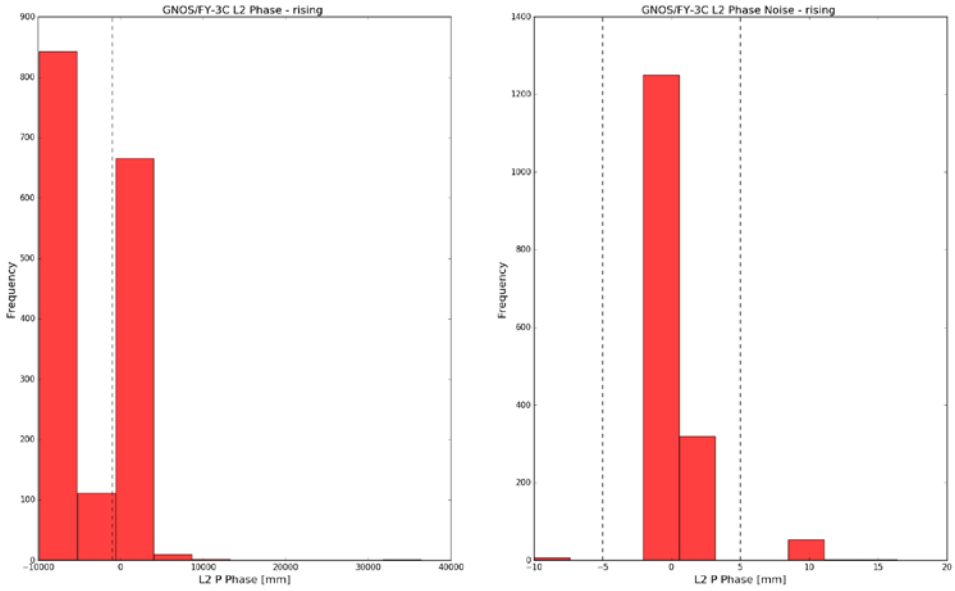

Figure 27. The histograms of L2 mean phase delay and its std. for the rising occultation using seven days of data from 16th Feb. to 22nd Feb 2017

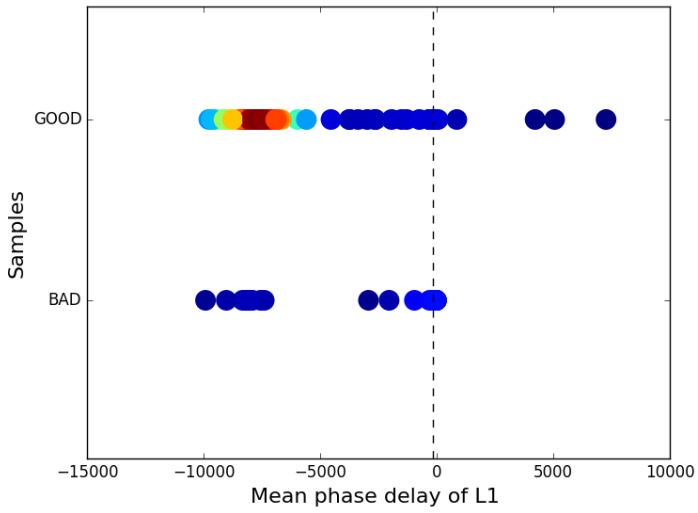

Figure 28. The L1 mean phase delay versus the good and bad samples (28th Jan 2017). Different colour represents different overlapping density, the dark blue is the lowest and the dark red is the highest, the colours between them show gradually higher density.

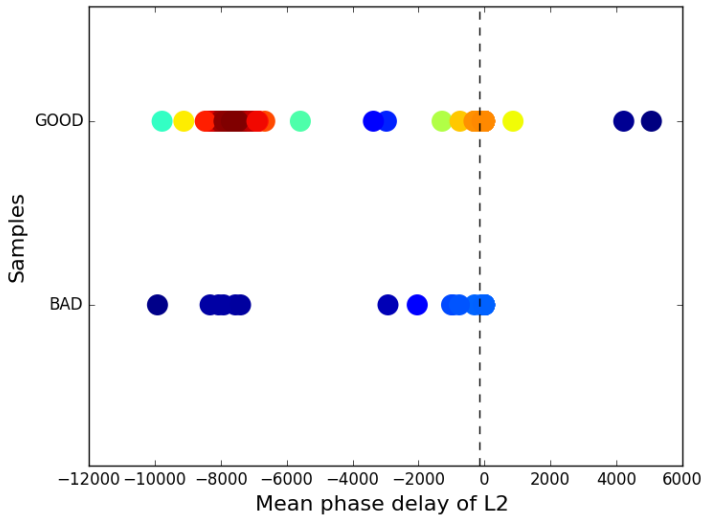

Figure 29. The L2 mean phase delay versus the good and bad samples (28th Jan 2017). Different colour represents different overlapping density, the dark blue is the lowest and the dark red is the highest, the colours between them show gradually higher density.

4.3 *L2_badness* from ROPP_PP

The L2_badness parameter from ROPP_PP is computed during the L2 correction using radiooptic analysis. It was originally proposed by Gorbunov (2005). It represents a quality indicator for L2 data. If the value of *L2_badness* is larger, the weighting of L2 phase data in the combination of L1 and L2 data should be smaller.

We tested the *L2_badness* to check if it is suitable to be a QC parameter for GNOS GPS-RO data. The histogram shows that the value of *L2_badness* is mostly smaller than 1000 (Figure 30). If we take 1000 as the threshold to identify GNOS profiles, about 6.3% of the profiles can be detected as bad. However, the actual ratio of the bad profiles is 9.7% in the samples for one day. About 3.8% profiles detected as bad ones by *L2_badness* parameter turn out to be normal or good profiles. However, about 6.8% bad profiles whose *L2_badness* values are lower than 1000. As Figure 31 shows, the *L2 badness* values of bad profiles ranges from 0 to 5000, and most of them are focused below 1000. Therefore, *L2_badness* may not be the most suitable QC parameter for GNOS GPS-RO data, and we do not suggest adopting it when carrying out the QC for GNOS GPS-RO data.

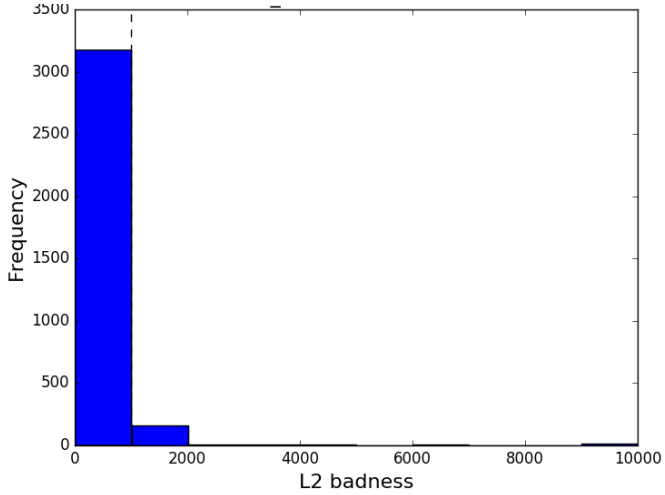

Figure 30. The histogram of *L2_badness* using seven days of data from 16th Feb. to 22nd Feb.2017

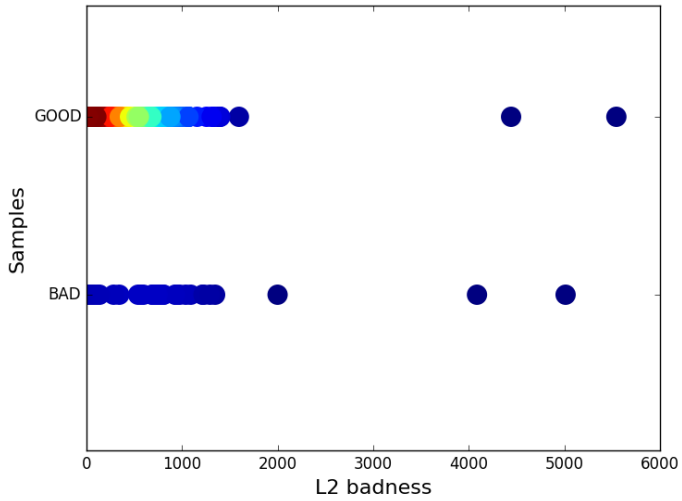

Figure 31. The *L2_badness* values vs the good and bad samples (28th Jan 2017). Different colour represents different overlapping density, the dark blue is the lowest and the dark red is the highest, the colours between them show gradually higher density.

4.4 Orbit height check

From Section 2.2, we find that there are some cases whose LEO orbit height changes significantly and this result in an ROPP routine hanging. It is necessary to check the normal height to screen out these cases. Normally, the LEO orbit height does not change significantly. We set the orbit height change threshold to 20 km; if this is exceeded the profile will not be processed. Besides the abrupt shift of LEO orbit, the latitude and longitude can change abruptly at the end of the occultation as well. Therefore, for an easier way to find the problem during the process of GNOS GPS-RO using ROPP, it can be checked through examining the variations of latitude and longitude for an occultation (Dr. Ian Culverwell personal communication).

4.5 The statistical performance of the applied QC methods

Although check six QC parameters have been investigated, we actually use the following three tests:

(1) If the occultation is rising, and the mean phase delays of L1 and L2 are greater than -150, the profile will be rejected;

(2) If the value of *noise_estimate* is greater than 20, the profile will be rejected;

(3) If the lowest SLTA of L2 is greater than 50 km, the profile will be rejected.

. These have been tested with one day of data. Firstly, the profiles are defined as good if the mean bias from the near surface to 50 km is within 5%. If not, it can be recognized as a bad case. Thus, the actual bad profiles using that standard account for about 9.7%. After applying the QC method, the total number of rejected profiles is 11.1%. The rate of correct identification is 82.7%, which accounts for 8.0% for the total samples. That means 3.1% profiles are mistakenly identified as the bad ones, and 1.7% of the profiles are still missing. In general, the performance of this kind of QC method can effectively identify most of the bad profiles.

5. Comparison with ECMWF forecast data

This section demonstrates the performances of the comparison between the observational GNOS bending angles and the simulated ones using ECMWF short-range forecast data. GNOS bending angle profiles are those which are carried out by the new L2 extrapolation and quality controls mentioned in section 3 and section 4, respectively. The time period is from 16th Feb. to 22nd Feb., 2017, with a total of 3069 profiles in seven days. ECMWF data used as the background is the state-of-art short-range forecast data with 137 vertical levels extending from surface to 0.01 hPa. Using the 2D bending angle forward operator, ECMWF forecast data can be simulated into the bending angle space.

GNOS observations are transformed into BUFR format with 247 vertical levels, which can be easily ingested in the operational system of ECMWF. To get better comparison, GRAS profiles from the same time period are also selected as a benchmark. Figure 32 displays the error statistics for the GNOS and GRAS bending angle profiles both separated into two different occultation directions, showing the relative standard deviation and relative bias of the two datasets. The relative standard deviation is about 1% at 10 – 35 km, increasing to about 12% at 50 km and more than 15% below 5 km impact height. Generally, the two datasets in terms of the relative standard deviation have similar error characteristics at most of the height, especially at the core range. The relative bias of the bending angle is almost the same below 20 km, but the rising and setting biases differ above 20 km, with the rising and setting occultations of GNOS have opposite sign of bias. Comparing the bending angle data before and after the new L2 extrapolation in Figure 33, the bending angle after the new L2 extrapolation performs better in relative standard deviation below 20 km. But the bias of the rising and setting is the same, implying that it is not introduced by the new L2 extrapolation method, and it existed in the original source. In theory, the bias of the setting and rising occultations should be the same. Processing during different steps of retrievals may introduce this bias, which needs to be investigated in the future.

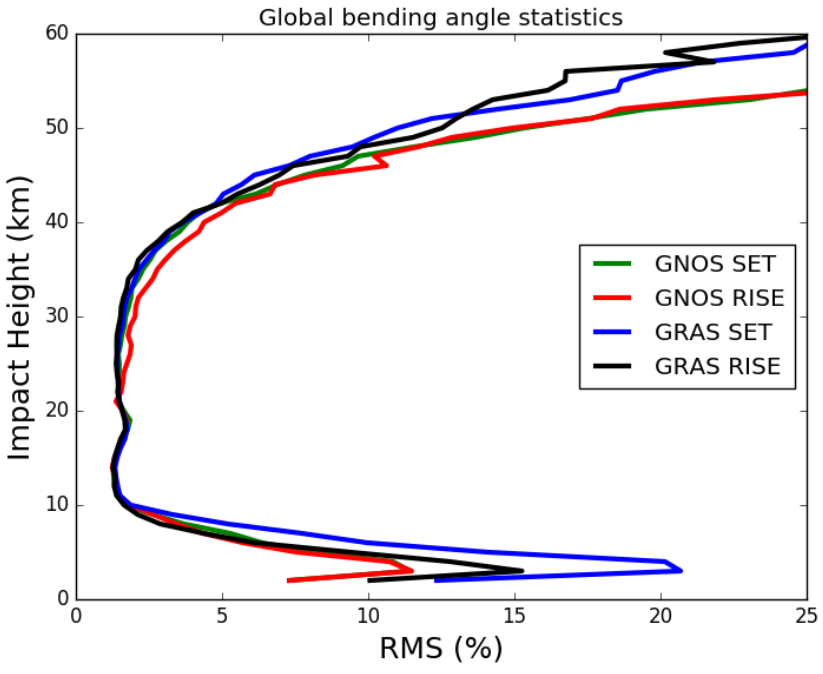

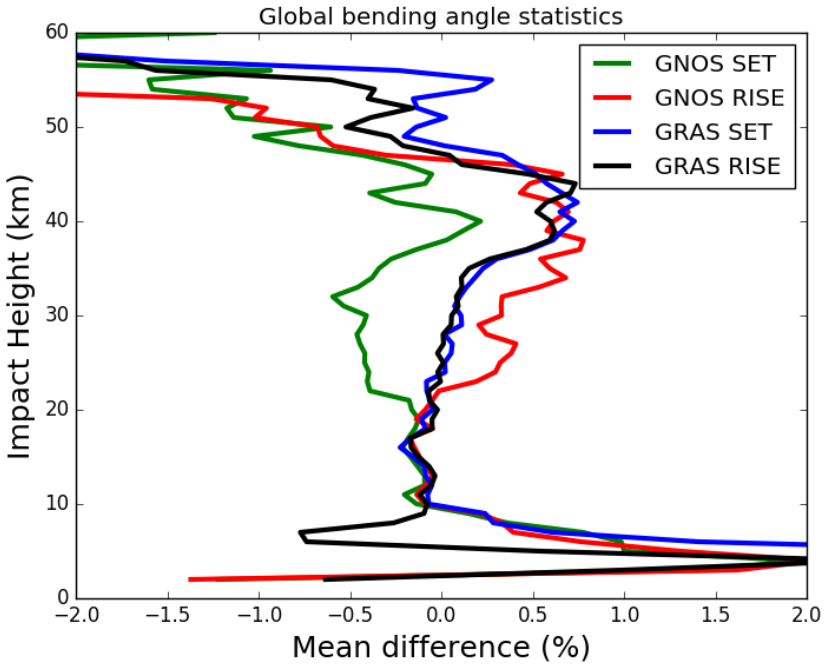

Figure 32. Global bending angle error analysis results, as a function of impact height, for the RMS (upper panel) and the Mean difference (lower panel). The green, red, blue and black lines are representative of setting occultation for GNOS, rising occultation for GNOS, setting occultation for GRAS and rising occultation for GRAS.

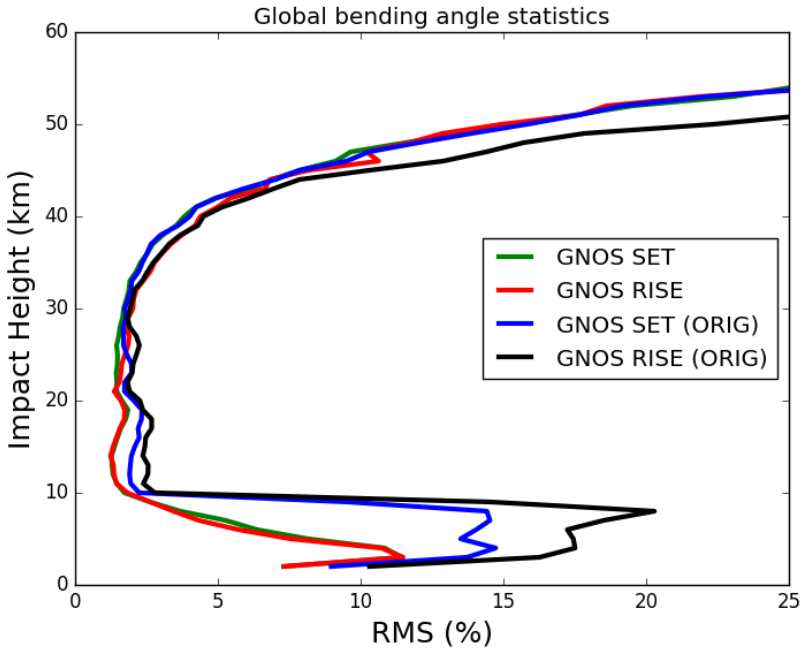

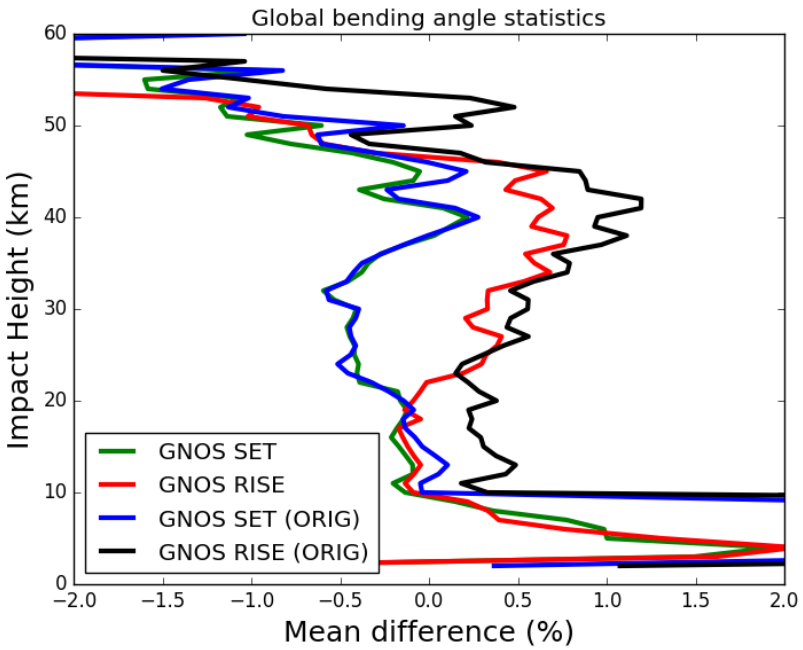

Figure 33. Global bending angle error analysis results, as a function of impact height, for the RMS (upper panel) and the Mean difference (lower panel). The green, red, blue and black lines are representative of setting occultation for GNOS after correction and QC, rising occultation for GNOS after correction and QC, setting occultation for GNOS before correction and QC and rising occultation for GNOS before correction and QC.

6. Conclusions and recommendations

6.1 Conclusions

This study focused on three main areas. First, perform a new L2 extrapolation for GNOS GPS-RO profiles. Second, find a suitable QC method for GNOS after applying the new L2 extrapolation. Third, evaluate the error statistics by comparing GNOS and ECMWF short-range forecast data. The main results can be summarized as following:

Firstly, we have identified and investigated the GNOS GPS-RO cases that fail quality control with large bending angle departures after the processing with the ROPP software. The large departures can be attributed to the GPS L2 signal tracking problems which stop above 20 km in terms of tangent height, and the related L2 extrapolation. The percentage of the profiles with large departure is about 13~15%. As a consequence, the main research question is focus on a better L2 extrapolation for GNOS when L2 signal stops above 20 km tangent height. Thus, a new L2 extrapolation approach is applied in the ROPP to solve the problem. The main procedure is at the bending angle space, which is based on the study of Culverwell and Healy (2016), introducing the corrected L2 bending angles produced by a Chapman layer model ionosphere and the fitting relationship between L1 and L2. We apply the approach to improve the L2 extrapolation of GNOS. The new method can effectively eliminate about 90% of the large departures. The remaining poor cases are mostly due to the L2 being completely missing.

Secondly, we have studied and established the quality control methods suitable for GNOS GPS-RO profiles after correcting the large departures. The new L2 extrapolation, *noise_estimate*, can be taken as a QC parameter to evaluate the performance of the extrapolation. It is the standard deviation of the difference between the fit and observations above the extrapolated height. Mean delay phases of L1 and L2 at the height of 60 to 80 km tangent height are analysed and applied in the QC as well. The lowest SLTA of L2 is also set as a threshold to identify the bad profiles. Furthermore, the orbit height, or the variation of latitude and longitude, for an occultation are checked to avoid cases where ROPP hangs, although the number of these cases are rather small. When examining the *L2_badness* parameter, which is introduced by ROPP software, we find that it is not the best internal quality control parameter for identifying the bad GNOS GPS-RO profiles, as it will result in higher ratio of bad profiles. Using the parameters mentioned above, the QC method can identify 82.5% of the bad profiles whose mean bias is greater than 5%.

Thirdly, we have assessed the quality of the GNOS bending angle by comparing with operational ECMWF short-range forecasts. GRAS profiles with the same time ranges are selected as a benchmark. The error statistics for the GNOS and GRAS bending angle profiles in terms of the relative standard deviation behaves similarly at most of the heights, especially at the core range. The relative bias of the bending angles are almost the same below 20 km, but it differs above 20 km, with the setting and rising occultations of GNOS having biases of opposite sign.. This needs to be investigated in the future.

In addition, we have transformed the GNOS observations into BUFR format with 247 vertical levels, which can be easily ingested into the operational system of ECMWF. This

guarantees the GNOS BUFR files distributed via GTS in the near future can be used by other NWP centers.

6.2 Recommendations

The VS activity also documents the GNOS specific problems using ROPP-PP and ROPP-FM modules, to guide future ROPP development. It is recommended that the ROM SAF should:

(1) Add more inspections for the GPS L1 and L2 excess phase/SNR, and examine their SLTA to assess their observational quality.

(2) Implement the new L2 extrapolation approach in bending angle space, introduced in the current study, for improving the L2 bending angle extrapolation. Furthermore, carry out more sensitivity tests for the optimal fitting ranges of L1 and L2.

(3) Examine the variations of the latitude and longitude for an occultation. Profiles with abrupt shift magnitude should be rejected because they cause ROPP retrievals to “hang”.

7. Acknowledgements

I have to express my sincere appreciation to Dr. Sean Healy, who gives me a lot of help not only in aspect of academy but also the English language, and unselfishly providing many ideas to solve some related problems. I also have to thank Christian Marquardt for his valuable suggestions with respect to the RO processing and QC methods. In addition, I want to thank Ian Culverwell and Chris Burrow for their discussions. At last but not least, I'd like to thank Kent Lauritsen and Steve English for giving me this chance to do the VS program and their kind help for my stay in ECMWF.

8. References

Anthes, R. A, Rocken, C., and Kuo, Y. H.: Applications of COS- MIC to meteorology and climate, Terrestrial Atmospheric and Oceanic Sciences, 11, 115–156, 2000.

Anthes, R. A., Ector, D., Hunt, D. C., Kuo, Y.-H., Rocken, C., Schreiner, W. S., Sokolovskiy, S. V., Syndergaard, S., Wee, T.- K., Zeng, Z., Bernhardt, P. A., Dymond, K. F., Chen, Y., Liu, H., Manning, K., Randel, W. J., Trenberth, K. E., Cucurull, L., Healy, S. B., Ho, S.-P., McCormick, C., Meehan, T. K., Thomp- son, D. C., and Yen, N. L.: The cosmic/formosat-3 mission: Early results, B. Am. Meteorol. Soc., 89, 313–333, 2008.

Ao, C. O., Hajj, G. A., Meehan, T. K., Dong, D., Iijima, B. A., Mannucci, J. A., and Kursinski, E. R.: Rising and setting GPS occultations by use of open-loop tracking, J. Geophys. Res., 114, D04101, doi:10.1029/2008JD010483, 2009.

Bai, W. H., Sun, Y. Q., Du, Q. F., Yang, G. L., Yang, Z. D., Zhang, P., Bi, Y. M., Wang, X. Y., Cheng, C., and Han, Y.: An introduc- tion to the FY3 GNOS instrument and mountain-top tests, At- mos. Meas. Tech., 7, 1817–1823, doi:10.5194/amt-7-1817-2014, 2014.

Beutler, G.: Methods of Celestial Mechanics, Springer-Verlag, Berlin, Heidelberg, New York, Germany, USA, ISBN 3-211- 82364-6, 2005.

Beyerle, G., 1. Wickert., T Schmidt, and C. Reigber (2004), Atmospheric sounding by GNSS radio occultation: An analysis of the negative refractivity bias using CHAMP observations, J Geophys.Res., 109, D01106, doi:10.102912003JD003922.

Beyerle, G., Schmidt, T., Michalak, G., Heise, S., Wickert, J., and Reigber, C.: GPS radio occultation with GRACE: Atmospheric profiling utilizing the zero difference technique, Geophys. Res. Lett., 32, L13806, doi:10.1029/2005GL023109, 2005.

Bi, Y.-M., Yang, Z.-D., Zhang, P., Sun, Y.-Q., Bai, W.-H., Du, Q.- F., Yang, G. L., Chen, J., and Liao, M.: An introduction to China FY3 radio occultation mission and its measurement simulation, J. Adv. Space Res., 49, 1191–1197,doi:10.1016/j.asr.2012.01.014, 2012.

Dach, R., Hugentobler, U., Fridez, P., and Meindl, M.: Bernese GPS Software Version 5.0. Astronomical Institute, University of Bern, Switzerland, 2007.

Gorbunov, M. E.: Ionospheric correction and statistical optimization of radio occultation data, Radio Sci., 37, 17-1–17-9, doi:10.1029/2000RS002370, 2002.

Gorbunov, M. E. and Lauritsen, K. B.: Analysis of wave fields by Fourier Integral Operators and their application for radio occultations, Radio Sci., 39, RS4010, doi:10.1029/2003RS002971, 2004.

Gorbunov, M. E., Lauritsen, K. B., Benzon, H.-H., Larsen, G. B., Syndergaard, S., and Sørensen, M. B.: Processing of GRAS/METOP radio occultation data recorded in closed-

loop and raw-sampling modes, Atmos. Meas. Tech., 4, 1021–1026, doi:10.5194/amt-4-1021-2011, 2011.

Hajj, G. A., Ao, C. O., Iijima,B. A., Kuang, D., Kursinski,E. R., Mannucci, A. J., Meehan, T. K., Romans, L. J., de la Torre Juarez, M., and Yunck, T. P.: CHAMP and SAC-C atmospheric occultation results and intercomparisons, J. Geophys. Res., 109, D06109, doi:10.1029/2003JD003909, 2004.

Healy, S. B. and Thepaut, J. N.: Assimilation experiments with CHAMP GPS radio occultation measurements, Q. J. Roy. Meteorol. Soc., 132, 605–623, doi:10.1256/qj.04.182, 2006.

I D Culverwell and S B Healy (2016). SAF/ROM/METO/REP/RSR/017: Simulation of L1 and L2 bending angles with a model ionosphere.

Kuo, Y.-H., Wee, T.-K., Sokolovskiy, S., Rocken, C., Schreiner, W., Hunt, D., and Anthes, R. A.: Inversion and error estimation of GPS radio occultation data, J. Meteor. Soc. Japan, 82, 507–531,2004.

Kuo, Y.-H., Schreiner, W. S., Wang, J., Rossiter, D. L., and Zhang, Y.: Comparison of GPS radio occultation sound- ings with radiosondes, Geophys. Res. Lett., 32, L05817, doi:10.1029/2004GL021443, 2005.

Kursinski, E. R., Hajj, G. A., Bertiger, W. I., Leroy, S. S., Meehan, T. K., Romans, L. J., Schofield, J. T., McCleese, D. J., Mel- bourne, W. G., Thornton, C. L., Yunck, T. P., Eyre, J. R., and Nagatani, R. N.: Initial Results of Radio Occultation Observations of Earth's Atmosphere Using the Global Positioning System, Science, 271, 1107–1110, doi:10.1126/science.271.5252.1107, 1996.

Kursinski, E. R., Hajj, G. A., Hardy, K. R., Schofield, J. T., and Lin- field, R.: Observing Earth's atmosphere with radio occultation measurements, J. Geophys. Res., 102, 23429–23465, 1997.

Ladstädter, F., Steiner, A. K., Schwärz, M., and Kirchengast, G.: Climate intercomparison of GPS radio occultation, RS90/92 ra- diosondes and GRUAN from 2002 to 2013, Atmos. Meas. Tech., 8, 1819–1834, doi:10.5194/amt-8-1819-2015, 2015.

Offiler, D.: The radio occultation processing package (ROPP) an overview, Tech. rep., GRAS SAF, Document-No: SAF/GRAS/METO/UG/ROPP/001, 2008.

Scherllin-Pirscher, B., Steiner, A. K., Kirchengast, G., Kuo, Y.-H., and Foelsche, U.: Empirical analysis and modeling of errors of atmospheric profiles from GPS radio occultation, Atmos. Meas. Tech., 4, 1875–1890, doi:10.5194/amt-4-1875-2011, 2011.

Shi C, Zhao Q, Lou Y. Recent development of PANDA software in GNSS data processing[J]. Proc Spie, 2008, 7285:231-249.

Sokolovskiy, S., Rocken, C., Schreiner, W., Hunt, D. C., and Johnson, J.: Postprocessing of L1 GPS radio occultation signals recorded in open-loop mode, Radio Sci., 44, RS2002, doi:10.1029/2008RS003907, 2009.

Spilker, J. J.: GPS signal structure and performance characteristics, Navigation, 25, 29–54, 1978.

Von Engeln, A., Healy, S., Marquardt, C., Andres, Y., and Sancho, F.: Validation of operational GRAS radio occultation data, Geo- phys. Res. Lett., 36, L17809, doi:10.1029/2009GL039968, 2009.

Ware, R., Rocken, C., Solheim, F., Exner, M., Schreiner, W., An- thes, R., Feng, D., Herman, B., Gorbunov, M., Sokolovskiy, S., Hardy, K., Kuo, Y., Zou, X., Trenberth, K., Meehan, T., Mel- bourne, W., and Businger, S.: GPS sounding of the atmosphere from lower Earth orbit: preliminary results, B. Am. Meteorol. Soc., 77, 19–40, 1996.

Wickert, J., Reigber, C., Beyerle, G., Konig, R., Marquardt, C., Schmidt, T., Grunwaldt, L., Galas, R., Meehan, T. K., Mel- bourne, W. G., and Hocke, K.: Atmosphere sounding by GPS ra- dio occultation: First results from CHAMP, Geophys. Res. Lett., 28, 3263–3266, 2001.

Yang, J., Zhang, P., Lu, N.-M., Yang, Z.-D., Shi, J.-M., and Dong, C.-H.: Improvements on global meteorological observa- tions from the current Fengyun 3 satellites and beyond, Int. J. Digital Earth, 5, 251–265, 2012.

Zou, X., and Z. Zeng (2006), A quality control procedure for GPS radio occultation data, J. Geophys. Res., 111, D02112, doi:l0.1029/2005JD005846.

9. List of Acronyms

BDS	BeiDou navigation System
CAS	Chinese Academy Science
CHAMP	CHAllenging Minisatellite Payload
CMA	Chinese Meteorological Administration
CT	Canonical Transform
COSMIC	Constellation Observing System for Meteorology, Ionosphere, and Climate
ECMWF	European Centre for Medium-range Weather Forecasts
EUMETSAT	EUropean organisation for the exploitation of METeorological SATellites
FSI	Full Spectmm Inversion
FY	Feng Yun
GNOS	Global Navigation Occultation Sounder
GNSS	Global Navigation Satellite System
GPS	Global Positioning System (USA)
GPS/Met	Global Positioning System/Meteorological
GRACE	Gravity Recovery and Climate Experiment
GRAS	GNSS Receiver for Atmospheric Sounding (on Metop)
GSN	Ground Service Network
GTS	Global Telecommunication System
IGS	International GNSS Service
LC	Linear Combination
LEO	Low Earth Orbit
Metop	Meteorological Operational Satellite
NetCDF	Network Common Data Form
NSMC	National Satellite Meteorological Center (China)
NSSC	National Space Science Center
NWP	Numerical Weather Prediction
PANDA	Positioning And Navigation Data Analyst
POD	Precise Orbit Determination
QC	Quality Control
RO	Radio Occultation
ROM SAF	Radio Occultation Meteorology (ROM) Satellite Application Facility (SAF) (EUMETSAT)
ROPP	Radio Occultation Processing Package
SAC-C	Satellite de Aplicaciones Cientificas-C
SLTA	Straight Line Tangent Altitude
SNR	Signal to Noise Ratio
TEC	Total Electronic Content